THE RELATIONSHIP BETWEEN PLATE CURVATURE AND ELASTIC PLATE THICKNESS: A STUDY OF THE PERU-CHILE TRENCH

by

ANNE VICTORIA JUDGE

B.A., Physics, Williams College
(1984)

Submitted to the Department of Earth,
Atmospheric, and Planetary Sciences
and to Woods Hole Oceanographic Institution
in Partial Fulfillment of
the Requirements of the Degree of
Master of Science in Earth Sciences

May, 1988

Signature of Author_____
Department of Earth, Atmospheric, and Planetary Sciences
May, 1988

Certified by_____
Marcia K. McNutt
Associate Professor, Marine Geophysics
Thesis Supervisor

Accepted by_____
Marcia K. McNutt, Chairman
Joint Committee in Marine Geology and Geophysics

THE RELATIONSHIP BETWEEN PLATE CURVATURE AND ELASTIC PLATE THICKNESS: A STUDY OF THE PERU-CHILE TRENCH

by

ANNE V. JUDGE

Submitted to the Department of Earth, Atmospheric, and Planetary Sciences
and to Woods Hole Oceanographic Institution
in Partial Fulfillment of the Requirements of the Degree of
Master of Science in Earth Sciences

ABSTRACT

The age of the Nazca plate where it enters the Peru and northern Chile trenches varies from 30 Ma in the north to 45 Ma in the south as its dip beneath the South American continent steepens from 13° to 30°. If the elastic thickness T_e of oceanic lithosphere depends only on its age, and therefore thermal state, we would expect that T_e determined from fitting the flexure of the lithosphere over the outer rise as revealed in the depth and geoid anomalies would increase from the Peru Trench in the north to the northern Chile Trench further south. We find that just the opposite is true: the lithosphere appears stiffer outboard of the Peru Trench than it does further south, and the isotherm controlling the elastic/ductile transition must be 600°C or greater if the thermal structure of the plate is that predicted by the standard thermal plate model. Because the decrease in plate stiffness to the south is correlated with a decrease in the minimum radius of curvature of the flexed plate over the outer rise and outer trench wall, we interpret our result in terms of inelastic yielding of the oceanic lithosphere when bent to high strains. The fact that the more highly bent segment of subducting lithosphere also dips at a steeper angle at greater depth beneath the continent might suggest that the amount of inelastic weakening of the lithosphere could be predicted from seismic images of the downgoing slab, but we find little support for this correlation worldwide. The forces and moments controlling the shallow deformation of the plate seaward of the trench do not appear to be linked to upper mantle processes which impose the dip at greater depth. Finally, we consider the possibility that the elastic thickness of the lithosphere would be reduced for trenches that are highly arcuate in map view, again due to inelastic yielding. If such a relationship exists, the effect for oceanic lithosphere is much smaller than what is documented for continental plates where they underthrust highly arcuate fold belts

Thesis Supervisor: Dr. Marcia K. McNutt, Associate Professor of Marine Geophysics

INTRODUCTION

It is generally agreed that oceanic lithosphere behaves as a thin elastic plate in response to applied stress over geologic time scales [*Walcott*, 1970; *Hanks*, 1971; *Watts and Cochran*, 1974; *Caldwell et al.*, 1976], and that the effective elastic thickness of the plate increases as the square root of age of the plate at the time of loading due to thermal control on the depth to the elastic/ductile transition [*Watts et al.*, 1980]. What is less certain is the magnitude of the reduction in the effective elastic thickness from the value predicted by lithospheric age due to inelastic processes within sharply bent plates at subduction zones, despite a number of attempts to explicitly include plastic deformation in flexural models [*Turcotte et al.*, 1978; *McAdoo et al.*, 1978; *Bodine and Watts*, 1979; *Carey and Dubois*, 1981] and the rheological arguments for its importance [*Goetze and Evans*, 1979; *McNutt and Menard*, 1982]. A better calibration of the yield strength of oceanic lithosphere is essential for understanding its rheology and state of stress.

The magnitude of the yield strength of oceanic lithosphere also bears on the problem of understanding the thermal structure of midplate swells which surround recently active hotspot volcanos. It has been known for at least a decade that the elastic plate thickness for old (>80 Ma) oceanic lithosphere flexed at trenches is about 30 km and is equal to that of old lithosphere loaded by active volcanos [*Watts and Cochran*, 1974; *Caldwell et al.*, 1976]. Two explanations have been proposed to account for this similarity:

(1) Inelastic yielding at the trenches is not important, and lithospheric reheating at midplate swells is either nonexistent or confined to great depth [*Watts et al.*, 1980; *Calmant and Cazenave*, 1988]. The 30-km plate thickness indicates that the isotherm controlling the elastic/ductile transition in oceanic lithosphere is 375–450°C.

(2) The isotherm controlling the elastic/ductile transition is 600°C or higher, but inelastic yielding reduces the elastic plate thickness at trenches compared to that predicted from the

depth of that isotherm [*McNutt and Menard*, 1982]. Midplate swells result from lithospheric heating, which raises the 600°C isotherm and thins the elastic plate relative to normal lithosphere of the same age [*McNutt*, 1984]. The effects of inelastic yielding at trenches, where strains are high but thermal anomalies unlikely, and of lithospheric reheating beneath swells, where strains are low but thermal anomalies suspected, happen to be of similar magnitude (about 10–20% reduction of the predicted elastic plate thickness in the absence of high strains or thermal perturbations).

Thus by determining the magnitude of inelastic yielding at trenches we can indirectly estimate the amount of lithospheric reheating beneath midplate swells.

The Peru-Chile Trench provides a suitable natural laboratory for investigating lithospheric rheology, for as the age of the subducted Nazca plate increases to the south along the trench system, the degree of deformation of the plate on the outer rise and outer trench wall increases to accommodate a more steeply dipping plate beneath South America. The area used in this study lies between latitudes 6°S and 25°S. Within this region the age of the plate increases approximately 15 my, from 30 Ma north of the Mendano Fracture zone, which enters the trench near 10°S [*Handschumacher*, 1976; *Hilde and Warsi*, 1984], to 45 Ma south of the Nazca Ridge, a large aseismic ridge which intersects the trench between 14°S and 17°S [*Herron*, 1972; *Scheidegger and Corliss*, 1981]. An abrupt change in the dip of the subducted slab has been observed near 16°S, from an average of 13° in the upper 200 km north of that latitude to approximately 30° to its south [*Barazangi and Isacks*, 1976; *Barazangi and Isacks*, 1979a]. Using observations of depth and geoid anomalies, we will examine what constraints can be placed on thermal and stress controls on effective elastic plate thickness, and their relative importance.

PLATE THEORY AND MANTLE RHEOLOGY

The lithosphere can be approximated as a thin plate overlying a fluid mantle. Such a plate will be deflected from its equilibrium position by external forces imposed on it. Treating such a plate in two dimensions, its displacement w at a point with no vertical load is described by

$$\frac{d^2M}{dx^2} - P\frac{d^2w}{dx^2} - \Delta\rho\, g\, w = 0, \tag{1}$$

where M is the bending moment, P is the horizontal load on the plate, $\Delta\rho$ is the difference in density between the underlying mantle rock and the overlying water, and g is the gravitational acceleration [*Caldwell et al.*, 1976; *Turcotte and Schubert*, 1982]. The bending moment is the integration of the torque acting on the plate over its cross-section, which can be written as

$$M(x) = \int_0^H (z - z_n)\cdot\sigma_f(z)\, dz \tag{2}$$

where H is the thickness of the plate, $\sigma_f(z)$ are the fiber stresses in the plate, and z_n is the depth of the neutral plane of bending [*McNutt and Menard*, 1982].

The simplest model consists of a plate which is perfectly elastic through its entire thickness. In this case (2) can be used to derive the expression

$$M(x) = -D\frac{d^2w}{dx^2} \tag{3}$$

where D is the flexural rigidity of the plate, defined as

$$D = \frac{E\, T_e^3}{12(1-\nu^2)} \tag{4}$$

where T_e is the thickness of the plate, E is Young's modulus, and ν is Poisson's ratio [*Turcotte and Schubert*, 1982]. Since the second derivative of the displacement of the plate at any point is the curvature K, (3) shows that moment is proportional to curvature in an elastic plate, with flexural rigidity as the constant of proportionality.

The curvature of a plate induces fiber stresses. In a downward bending plate these are tensional near the surface and compressional near the base. In a perfectly elastic plate, the fiber stresses increase with distance from the neutral axis of bending, as shown in Figure 1a. As curvature increases, the maximum elastic stress that must be supported increases. However, all known rocks have an elastic limit, such that as the stress reaches a critical value, the rock will yield [*Goetze and Evans*, 1979; *Brace and Kohlstedt*, 1980; *McNutt and Menard*, 1982].

The stress at which failure occurs is dependent on temperature and pressure, and therefore on depth. Two primary modes of failure occur. At shallow depths, under low temperature and pressure, lithospheric material is brittle and fails by fracture and by slippage along preexisting fractures. Evidence suggests that sufficient cracks exist in the lithosphere that the magnitude of stress which can be supported before failure occurs is controlled by frictional resistance to slippage [*Goetze and Evans*, 1979; *Brace and Kohlstedt*, 1980]. In this region strength increases with depth in a linear manner. Deeper in the lithosphere failure occurs by ductile creep and as depth increases creep occurs at lower stresses. The base of the mechanical lithosphere, at depth T_m, is defined as the depth at which only a negligible stress difference can be supported on geological time scales [*McNutt*, 1984]. The stress at which failure occurs defines a yield envelope, which can be approximated by the outer line in Figure 1b. Within this region in the stress-depth plane, rock mechanics data indicate that lithospheric material has high strength and displays elastic behavior. A bent lithospheric plate will therefore behave elastically at intermediate depths where curvature-induced stress is small and the plate is strong, but will experience failure near its surface and base, where curvature has the largest effect and the plate is weakest.

The distribution of stress with depth in such a plate is shown by the slanted inner line in Figure 1b.

From Equation (2) it can be seen that the bending moment of such a plate will be smaller than that of a perfectly elastic plate of the same thickness, which has larger stresses through its depth. Since the bending moment controls the deflection of a plate, the plate thickness found from a bathymetric profile assuming perfectly elastic rheology will underestimate the true mechanical thickness of the lithosphere. *McNutt* [1984] has shown in graphical form the relationship of elastic to mechanical thickness as a function of curvature and horizontal load P, by equating the moment of an elastic plate, which can be calculated analytically from (1), to that of a plate of more realistic rheology, calculated using (3). These show the reduction in apparent elastic thickness as curvature increases. When curvature is small, failure occurs through a small depth, and the elastic thickness varies little from the mechanical thickness. When curvature is large, the mechanical thickness is considerably less than the apparent elastic thickness; for a curvature of 9×10^{-7} m^{-1}, T_e is near 2/3 T_m. Since curvature is not constant along a flexed plate, but changes with position, the effective elastic thickness will also change with position along the plate.

DATA : THE PERU-CHILE TRENCH

In order to study behavior of the plate seaward of the Peru-Chile Trench, bathymetric data on a 5-minute grid were used [*Heirtzler and Edward*, 1985]. Maps showing the location of the areas for which data were obtained and contours of bathymetry are given in Figure 3. The gridded data were interpolated from shipboard readings along tracks that provide generally good coverage of the area, with separations parallel to the trench usually less than 30 km, whereas characteristic shapes of structures in that dimension in most cases can be traced over 80 km. We interpolated the bathymetric data onto profiles spaced at 10-

km intervals perpendicular to a number of line segments fit to the trench axis. An attempt was made to apply an age correction to the profiles thus obtained, but they had no apparent slope with age despite the young age of the crust.

These profiles were fit by the simplest solution to the equation for the deflection of a perfectly elastic plate. This solution, found by neglecting the compressional term in Equation (1), making the substitution for bending moment indicated by Equation (3), and placing the origin at the first point of zero deflection seaward of the trench axis, is of the form

$$w(x) = A\, e^{-\frac{x}{\alpha}} \sin\frac{x}{\alpha} \tag{5}$$

where $\alpha^4=(4D/\Delta\rho g)$ and A is a constant which controls the amplitude of the solution [*Turcotte et al.*, 1978; *Jones et al.*, 1978; *Turcotte and Schubert*, 1982]. By fitting elastic curves representing a number of elastic thicknesses to each bathymetric profile, the rms (root mean square) misfit was accumulated as a function of elastic thickness, allowing the best-fitting profile to be determined.

We quantify the quality of the fit by measuring one-half the width of the misfit vs. elastic thickness curve where the misfit reached 1.5 times its minimum value. This width is dependent on both the slope of this curve and the minimum value the misfit obtains. A profile which is fit with only a small misfit and a profile fit with a large misfit but a steep curve (Figure 2) can both be considered to have a well-constrained elastic thickness and will both have a narrow half-width as determined by this method. Profiles for which the half-width was less than 10 km were considered to have a well-constrained value for T_e.

The loads experienced by the plate beneath the inner trench wall, which produce this profile, can be reduced to a shear load V_o and a bending moment M_o acting on the cross-section of the plate at the trench axis. The bending moment was calculated according to (3), and the shear load is its first derivative. The stresses imposed on the plate by its bending

are indicated by its curvature K, the second derivative of the deflection. The values of shear load and moment at the trench axis and curvature at the origin were determined for the elastic profile which best fit the observed profile. The advantage of calculating the curvature K at the first zero crossing seaward of the trench axis is that the relationship between moment and curvature is independent of any applied in-plane stress P [*McNutt and Menard,* 1982].

Additional information was gained from consideration of geoid heights across the region. Geoid data were obtained on a 15-minute grid [*Marsh et al.*, 1986] and interpolated onto profiles spaced 30 km apart, corresponding to every third bathymetric profile across the trench axis. The reference geoid (GEM 9) was removed to degree and order 10, but a long-wavelength variation was still apparent across the region of interest. This trend did not appear to relate to the topography of the outer rise and trench, and its slope was greater than that of the geoid-age relationship in young crust. It was removed by subtracting from each profile a line of constant slope. These geoid profiles were used to find the elastic parameters for the plate which best reproduced the geoid, and also served as an aid in determining the degree to which features in the bathymetric profiles were flexurally supported.

To model the geoid of an elastic plate, equation (5) was applied to define the surfaces of a simple seven-kilometer-thick slab of constant density overlying a denser mantle, and the resulting geoid was generated using the method developed by *Parker* [1972]. This model of the slab is consistent with the results of seismic and gravity studies of the area [*Fisher and Raitt*, 1962; *Hayes*, 1966; *Ocala and Meyer*, 1973]. Allowing the density increase from the surface to the Moho to occur across several crustal layers as indicated in these studies has no apparent effect on the resulting geoid, and so was not included. Since the slope of the Moho under the continental plate is not easily found, the mass distribution landward of the trench axis was approximated by reflecting the profile about this point, an approach used by *McAdoo and Martin* [1984]. The geoid profiles resulting from this approximation were

in good agreement with the observed geoid above the trench wall, the region of the geoid which is most sensitive to the slope of the Moho under the continent.

The geoid can be used as an aid in distinguishing between compensated and flexurally-supported topography because depth variations caused by local irregularities in crustal thickness should be locally compensated with a small geoid signal, while flexurally supported topography, with no such compensation, produces a large geoid signal. Geoid profiles were generated for a slab with boundaries defined by the observed bathymetry and a parallel seven-kilometer-deep Moho. Large compensated features could be identified by comparing these profiles to observed geoid heights.

RESULTS

First we will present the results from modeling the depth and geoid data from the Nazca plate seaward of the Peru and northern Chile trenches assuming two-dimensional flexure of a plate with constant rigidity and no applied in-plane stress as given by Equation (5). Enough profiles are adequately fit under these restrictive assumptions to estimate the elastic plate thickness and plate curvature in each area. However, at the end of this section we do discuss the effect of relaxing these assumptions to allow variable plate rigidity, three-dimensional bending, and horizontal thrusts.

Peru

The Peru trench can be approximated as two line segments, a 300-km long northern segment running from 6°S and 8.5°S and a 600-km long southern segment continuing to 13.2°S, where the trench becomes shallower and less well-defined approaching the flanks of the Nazca Ridge. The region, including the areas defined by these segments of the trench, is shown in Figure 3b. Some representative bathymetric profiles crossing the trench are shown in Figure 4, and the geoid profiles along the same tracks appear in Figure 5. The bathymetric profiles are numbered consecutively from north to south within each

region. Those profiles which could be fit by elastic theory are shown with the best-fitting elastic curve superimposed. Geoid height profiles are identified by the number of the corresponding bathymetric profile, and are shown in Figure 5 with the best-fitting geoid profiles generated from elastic bathymetric curves.

An outer rise is apparent in all of the bathymetric profiles from the northern region and many from the southern region, although often its shape departs from the predicted decaying sinusoid of (5). Approximately half of the profiles in the northern region can be reasonably fit by elastic profiles, but only seven of the 60 profiles in the southern region produce reasonable fits. The elastic thickness, bending moment (counterclockwise, tending to increase the downward curvature of the plate) and load at the trench (positive downward), downward curvature at the zero crossing, and rms misfit for these profiles across the Peru trench are given in Table 1. Elsewhere in both regions profiles display rough topography unrelated to elastic flexure or bulges which are elongated compared to the elastic prediction. In the northernmost 250 km of the southern region, the outer rise is small or nonexistent, and its disappearance cannot be explained by sediment thickness patterns [*Hussong et al.*, 1976; *Dang*, 1984].

Those bathymetric profiles which could be fit are clustered into three groups: the five profiles intersecting the trench at the northernmost end of the northern segment, between 6°S and 6.4°S; profiles 11–21 of the same region, which cross the trench 60 to 160 km south-southeast of this, between 7°S and 7.7°S; and profiles 6–12 of the southern segment, crossing the trench between 9°S and 9.4°S. Except for the first profile, the first group is fit very well by elastic profiles (Figure 4a). The elastic thickness appears to decrease steadily from north to south. This characteristic may be explained in part, but not entirely, by the along-strike curvature of the trench as the end of the nearly linear segment is reached at the northern end, since as the angle at which the profile crosses the outer rise decreases from 90° the outer rise appears wider and the elastic thickness appears correspondingly larger. The profiles of the second group were also fit with relatively small misfit, but display a

systematic discrepancy from the theoretical profiles, with a more gradual rise to the outer bulge to seaward and a steeper slope on the trench wall than that due to a purely elastic curve (Figure 4c). The six profiles in the third group are near the southern segment's northern edge, in the area characterized by a small outer rise (Figure 4g). The thickness of the elastic plate which best fit this group of profiles averages 10 km, far smaller than the average elastic thickness of 28 km found for profiles throughout the northern region.

The geoid in the Peru province shows a consistent high above the outer rise. This high appears even over the part of the southern region where there is no outer rise in the bathymetry, and reaches its greatest height in the center of the southern region, where the bathymetric rise is large but elongated (Figures 4i,j and 5i,j). Nearly all of the observed profiles could be fit by an elastic model, with the results summarized in Table 2. The average elastic thickness is 38±3 km. However, near the northern edge of the southern region the Mendano Fracture Zone intersects the trench, with an associated change in crustal age of 12 Ma. Averaging values of elastic thickness found for same-age crust results in a value of 35±2 km for the 30 Ma lithosphere of the northern region and 39±3 km for the 42 Ma lithosphere south of the fracture zone. This value for the northern region is considerably larger than the value arrived at from the corresponding bathymetric profiles. The elastic thickness found south of the fracture zone cannot be compared results of modeling the bathymetry, since no bathymetric profiles in that area could be fit. Average curvatures are 1.7×10^{-7} m^{-1} in both areas, with a standard deviation of 0.1×10^{-7} m^{-1} in the north and 0.2×10^{-7} m^{-1} to the south. The elastic curves which generate the best-fitting geoid height profiles nearly always have longer, lower outer rises than are observed in the bathymetry. This is particularly true for profiles 13–29 of the northern region, where the outer rise of the profile which fits the bathymetry is over 8 times the height of that of the elastic profile which recreates the geoid (Figure 6). However, the height of the bulge in the elastic profiles which recreate the geoid is much more consistent between profiles than the observed heights of the outer rise, and where the outer rise observed in the bathymetry is

very small, the elastic profile associated with the best-fitting geoid profile displays a large rise.

Some of the observed geoid height profiles could also be satisfactorily fit by profiles generated from the observed bathymetry, assuming that it is paralleled by the Moho. This indicates that the observed bathymetry along these profiles may be a flexurally supported, but no such bathymetric profiles could be fit by elastic theory. Among the profiles shown here, this is so for profiles 10, 22, and 28 of the northern region and profile 40 in the south (Figures 4c,e,f,j). Geoid profiles generated from those southernmost profiles with very large, elongated outer rises (Figure 4k,l) and from profiles 13-19 of the northern region (Figure 4d) are much higher over the outer rise than is the observed geoid along those profiles (Figure 5d,k,l), implying that these large rises may be partially compensated. On the other hand, those bathymetric profiles with very low or nonexistent outer rises (Figure 4b,g) cannot be used to generate geoid height profiles with any high over the outer rise (Figure 6b,g). This inconsistency between the small value for elastic thickness obtained from the bathymetry and the presence of a distinct geoid high indicates that the bathymetry does not reflect the behavior of the plate, and for this reason values from the southern region were excluded in computing the average elastic thickness in the Peru province as found from the bathymetry. The average elastic thickness of the remaining profiles is 28±4 km, and the curvature of the plate at the first zero crossing averages $(2.8\pm0.4)\times10^{-7}$ m^{-1}.

North Chile

The trench off northern Chile, from the Nazca ridge to 25°S, consists of two relatively straight segments separated by a short region of extremely sharp curvature. This curved segment, which in map view has a radius of curvature of 310 km, can be approximated by three short straight segments. The area around the trench and the regions defined by the segments are shown in Figure 3c. The five regions are numbered from north to south as

they cross the trench, and within each region the profiles are numbered consecutively from north or northwest to south or southeast. Region 1 includes the northwest-southeast-trending 410-km-long portion of the trench lying immediately to the southeast of the Nazca ridge. The change in the dip of the slab occurs in the northwestern end of the region [*Barazangi and Isacks*, 1976; *Barazangi and Isacks*, 1979a]. In all of the profiles from the northern four of the five regions an outer bulge is apparent, reaching heights of over 1000 m in some cases. The fifth segment of trench in the northern Chile region is 480 km long, extending nearly due south. In this region, except at its northern edge, the outer rise is very rough, with ridges paralleling the trench near the region of the outer rise sometimes obscuring the bulge, due in part to an aseismic ridge which intersects the trench there at an angle of approximately 45°. Some bathymetric profiles from the region are shown in Figure 7, and the corresponding geoid profiles are shown in Figure 8.

The elastic thickness, bending moment and load at the trench, curvature at the first zero crossing, and rms misfit for the profiles which could be satisfactorily fit by an elastic model are given in Table 3. The great majority of these profiles were located in or slightly to the northwest of the area where the trench curves sharply, between 17.5°S and 21°S. Here the bulge is very high, over 1000 meters in some profiles, with a narrow peak and steep trench wall (Figure 7e–h). This shape represents a systematic deviation of the bathymetry from the theoretical elastic curves similar to that observed in profiles crossing the Peru trench near 7.5°S. Northwest of this, in the northern half of region 1, only two profiles could be fit by the elastic model (Figure 7a–c), and to the south, in region 5, only four profiles at the region's northern edge could be fit (Figure 7j–l). The average elastic thickness found for those profiles which were fit was 22±2 km. The curvature at the first zero is near 5×10^{-7} m^{-1} in the profiles across the relatively straight section of the trench lying to the north of the bight and increases to over 13×10^{-7} m^{-1} in the profiles across the most curved section of the trench, averaging $(12.4 \pm 2.6) \times 10^{-7}$ m^{-1}.

The geoid in the North Chile province shows a high corresponding to the outer rise throughout the region, and like the bathymetric rise it reaches its greatest height in the area where the trench curves sharply. The elastic thickness and other parameters describing those profiles which could be fit by elastic theory are given in Table 4, and Figure 8 shows geoid profiles from the region plotted with the best-fitting profiles generated from elastic curves. However, nowhere in the North Chile region can the geoid be as well fit by the elastic model as can the geoid in the Peru province. In the vicinity of the bight, where the bathymetry can be most successfully modeled by an elastic curve, profiles of the geoid height are characterized by a high over the outer rise with a relatively long, flat slope to seaward and a steep drop to landward of its peak—features which cannot be duplicated using an elastic model (Figure 8e–h). However, this region is the only area in which the values of elastic thickness derived from geoid height profiles match the values determined by reproducing the bathymetry. The average elastic thickness here is 24±2 km, and curvature averages $(6.7\pm1.5)\times10^{-7}$ m^{-1}.

Geoid profiles were generated from the observed bathymetry with mixed success. The technique of approximating the mass distribution landward of the trench axis by mirroring the seaward bathymetry, which was used with great success in the Peru province, does not appear to give good results here, the descent into the trench apparently being too abrupt. Instead the Moho was assumed to descend at a constant slope under the continent. Some profiles in the vicinity of the bight can be better fit by a geoid height profile thus generated from the observed bathymetry than by profiles generated from an elastic curve (Figure 9), but the vast majority could not be fit this way. The result of thus modeling profiles in region 5, assuming that the observed bathymetry is uncompensated, is a calculated geoid much larger than that observed, confirming the conclusion drawn from the bathymetry that large crustal features, possibly related to an aseismic ridge, are masking any elastic response to entering the trench.

The sharply downbent and thinned portion of the plate in the North Chile province coincides with two features of the subduction zone which might possibly be linked to its extreme curvature and small elastic thickness. In this region the plate dips more steeply beneath the overriding plate than it does to the north, and the trench has unusually sharp curvature in map view. Below we discuss the possible significance of these correlations.

Elastic Plates with Variable Rigidity

If indeed inelastic processes caused by curvature-induced stresses have produced failure in the plate, one would not expect the bathymetric profiles to be completely described by an elastic profile with constant flexural rigidity. A look at those bathymetric profiles best fit by elastic theory shows that this is the case. In both regions many of these profiles display a systematic deviation from the theoretical curves, with a more gradual slope to seaward of the bulge and a steeper slope landward of the peak than predicted by elastic theory. This often results in the observed position of the peak of the bulge being offset to landward of its predicted position. When the best-fitting profile wrongly predicts the position of the bulge it also predicts an upward load at the trench axis, a result which is inconsistent with the expected forces on the plate. The ability to model the geoid in the region of the Chile bight by assuming that the Moho parallels the observed bathymetry further indicates that the shape of the rise may be the flexurally-maintained response of the plate with nonuniform rigidity to the applied load and moment rather than the result of preexisting topographic irregularities superimposed on an elastic response.

The observed shape of these outer rises appears consistent with a model of a stiff plate which is weakened as it reaches the peak of the bulge. In order to model this effective thinning of an elastic plate brought on by failure, Equation (1) can be solved for a plate in which the flexural rigidity D is assigned a lower value on the trench wall than on the ocean floor. Since the shape of the bathymetric and elastic profiles diverge at or near the peak of the outer rise, which is also the area at which the curvature begins to increase, this peak

was chosen as the point at which to change the value of the rigidity in this test. The rigidity seaward of this point was derived from the flexural rigidity and curvature at the origin of the best-fitting elastic curve by predicting the rigidity if no curvature and thus no thinning due to failure were present [*McNutt*, 1984], while the rigidity to landward and the exact position of the change in rigidity were chosen to best fit the observed profile. The results are shown for a profile off Peru in Figure 10a and for a profile off northern Chile in Figure 10b. The shape of the bulge can be reproduced successfully by this method, although an end load sufficient to reproduce its height produces excessive slope in lower portions of the trench wall, near the trench axis. The degree of thinning which best fit the plate varied between the regions. In Peru the plate was best fit by an elastic thickness 5 km smaller landward of the bulge than to seaward, a decrease of 16%, whereas in northern Chile the plate was best fit by a model which thinned by more than a factor of two.

The fit on the lower trench wall could be improved in the Chile region by modeling the bathymetry with an elastic plate which is thinner at the peak of the bulge than on the seafloor, but then thickens again along the outer trench wall (Figure 10c). However, this model requires that the flexural rigidity of the plate increase from the peak of the bulge to the trench wall, an area where the curvature is increasing and where it would be expected that flexural rigidity would decrease. Several observations, including the presence of thrust faulting near the base of the trench wall [*Schweller et al.*, 1981] and a thickening of the plate approaching the trench axis [*Hussong et al.*, 1976], may help explain the appearance of a stronger plate here. The 5° spacing of the bathymetric data makes resolution of faults impossible, and since the data is interpolated onto this spacing from ship track data sharp features such as faults are smoothed in the process. Another possible explanation for this steepening, the accumulation of a wedge of sediments on the plate near the trench axis, appears to be ruled out by seismic cross-sections of the trench wall which indicate that sediment thickness remains constant from the outer rise nearly to the trench axis [*Schweller et al.*, 1981].

The values of elastic thickness found earlier by considering each profile to be of constant rigidity can be considered weighted averages of the true elastic thickness along the length of the profile. These values, compared to the values found by modeling the profile with one change in flexural rigidity, are smaller than the elastic thickness on the seafloor where no failure would be expected, but larger than that on the trench wall, near the zero-crossing. The values found when flexural rigidity is varied are similarly averages, but over smaller, arbitrarily chosen segments of the plate. At the Peru trench, profile #16 of the northern region is best fit by a constant 31.6-km-thick plate, or by a plate which changes in thickness from 32.8 and 27.6 km. Off northern Chile, profile #4 of region 2 is fit by a plate with a constant thickness of 21.5 km or by one which changes from 36.6 to 17.0 km. As the goal of this study is to understand the relationship between curvature-induced stresses and apparent elastic thickness, we wish to know if the curvature obtained by any elastic model is consistent with the plate thickness found according to that model at the point where curvature is measured. The curvatures of the profiles modeled here with variable rigidity were approximately 1.6 times their curvatures in Tables 1 and 3. This amount of change in curvature is consistent with the variation in elastic thickness at the zero-crossing as found by the two models [*McNutt*, 1984]. Therefore the values of elastic thickness found in this study should reflect the amount of thinning that the lithospheric plate is expected to undergo when it is bent to the calculated curvature.

Effect of In-Plane Stresses

In addition to a simple thinning of the plate with increasing curvature, other factors may influence the shape that it assumes. One possible factor is horizontal compression acting on the plate. This stress appears in the second term in Equation (1), and it primarily affects the state of stress in the plate, though when large enough it can affect the plate's shape. Including it in the calculation of perfectly elastic profiles has little discernible effect on the shape of the peak of the outer rise, but does increase the curvature in the lower part of the

trench wall. However, to accomplish this the compressional stress must be greater than 10^6 MPa, which is urealistically large. To accurately consider the effect of such stresses, a more realistic rheology which includes failure must be considered. In such a plate, even where there is no curvature, horizontal loading causes failure at the surface and base of the plate, so the plate has a smaller effective elastic thickness. *McAdoo and Sandwell* [1985], in a study of the buckling of the lithosphere under the Indian Ocean, have found that large compressive forces there have reduced the thickness of the elastic core of the plate to near one-tenth its full thickness. When curvature is added to a plate under such loading, the degree of failure differs from that of a plate which is not prestressed. A plate under 100 MPa of tension shows additional weakening with curvature of approximately the same amount as one without horizontal loading, but initially appears weaker; a plate under a similar amount of compression appears not to weaken as much [*McNutt*, 1984]. However, the effect of compression appears primarily in the measured thickness of the plate, not in the shape it assumes. Since the curvature of the bent plate is characterized by the remaining elastic core [*McAdoo and Sandwell*, 1984], we consider an elastic model a valid approximation of lithosphere entering a subduction zone, with horizontal loading serving to introduce a margin of uncertainty in the interpretation of the apparent elastic thickness of the plate in terms of a mechanical thickness.

Three-Dimensional Effects

In the region of the Chile bight, where the strike of the trench changes over 45° within 175 km, the sharp turn in the trench may be affecting the shape and amplitude of the outer rise. The rise reaches peaks of over 1200 m, far larger than most outer rises, which are rarely larger than 600 m [*Caldwell et al.*, 1976; *Turcotte et al.*, 1978; *Jones et al.*, 1978; *Carey and Dubois*, 1981]. The bulge also has a gravity high of 80 mgal associated with it, which is larger than those observed over any other Pacific trench [*Schweller et al.*, 1981]. In the case of this much surface curvature in a trench, an approximation which treats it as a

line load may not be valid. However, treating the trench as a cylindrical load of radius 350 km, using equations developed by *Brotchie* [1971], did not yield very different results than did our earlier modeling (Figure 11). The elastic curve thus derived which best fit a profile off northern Chile appeared nearly identical to the best-fitting curve derived assuming a line load (Figure 11b). The elastic parameters were slightly different in this case, with the elastic thickness which produced the best-fitting cylindrical curve 1.5 km smaller, but this fell within the range of uncertainty in the elastic thickness determined earlier. It appears that if the sharp curvature of the trench has any effect on the shape of the plate it cannot be modeled simply by changing the geometry of the load, and such complications can be safely ignored in favor of the model of a the two-dimensional line load.

Profiles Without Elastic Flexure

This discussion of means to better fit those bathymetric profiles which could be explained by the elastic model neglects the majority of profiles which could not be fit because of irregular bathymetry in the region of the outer rise. In some of these profiles the seafloor is rough well to seaward, and it appears that the topography on the outer rise is a continuation of these features. However, in many profiles the seafloor is smooth to seaward, yet the outer rise displays uneven topography apparent on a 10-km grid. *Erlandson et al.* [1981] have observed a region of rough basement along the entire area of the Peru-Chile trench included in this study, extending 300 km seaward from the trench axis. The region shows evidence of faulting, upper crustal deformation, and volcanics, extending farther seaward than does the extensional faulting on the trench wall. They attribute these features to stresses encountered by the plate as it approaches the subduction zone. This disruption and failure of the crust may mask or prevent elastic behavior of the plate producing the bathymetry apparent in these rough profiles.

DISCUSSION

Temperature at the Elastic/Ductile Transition

The results from Peru and North Chile can be used to test several thermo-mechanical models of oceanic lithosphere. Along the Peru trench, where the curvature of the plate is lower and therefore inelastic yielding should be less significant than further south, the average elastic thickness of the 30-my-old plate as found from the bathymetry is 28±4 km. If inelastic yielding can be completely ignored here and if the thermal structure of the Nazca plate in this region corresponds to the standard thermal plate model of *Parsons and Sclater* [1977], then these value of elastic plate thickness can be used to estimate the temperature at the elastic/ductile transition. For 30 Ma lithosphere, the *Parsons and Sclater* [1977] model predicts about 700±85°C at a depth of 28±4-km. If there is any inelastic yielding, then the actual depth to the elastic/ductile transition would be even greater, and the temperature even higher. A lower temperature at the transition, such as 450°C [*Watts et al.*, 1980] or 400°C [*Calmant and Cazenave*, 1988] would only be consistent with the data from the Peru Trench if the thermal structure of the Nazca plate is significantly colder than usual. The regional depth offshore Peru, however, is 4500 m, which is near the predicted value for normal 30-Ma lithosphere. Therefore, we doubt the existence of negative thermal anomalies and conclude that the isotherm controlling the brittle/ductile transition is at least 615°C.

The much colder estimates of the temperature at the base of the elastic plate from *Watts et al.* [1980] and *Calmant and Cazenave* [1988] were either principally or exclusively derived from observations of elastic plate thickness beneath midplate volcanos. In such studies, it is the thickness of the plate which is "observed", and in converting plate thickness to the temperature at the base of the plate they must adopt some geotherm, which in these cases was that of the standard thermal plate model. We believe that the assumption of a standard geotherm in regions of hot spot activity is inappropriate, and that the elastic plate thicknesses mark the depth to an isotherm much nearer 700°C, which is simply

elevated beneath the midplate volcanos. Of course there is some uncertainty in our estimate of T_e for the Peru Trench (Tables 1 and 2), but even the scatter in the data does not permit elastic plate thicknesses as low as 15 to 17 km in order to match the predicted depth to the 400–450°C isotherm.

Values of elastic thickness derived by modeling the geoid are considerably greater than those which fit the bathymetry, and suggest a much hotter temperature controlling the brittle/ductile transition. At the depth of the calculated base of the 30 Ma plate of the northern Peru region, 35±2 km, the temperature is expected to be near 840±35°C, and at 39±3 km in 42 Ma lithosphere it should be near 800±50°C. Similar results were obtained by *McAdoo and Martin* [1984] and *McAdoo et al.* [1985], who modeled geoid data over nine trenches and concluded that the thickness of the mechanical lithosphere is approximately defined by the 740°C isotherm. At nearly all trenches covered by their study the geoid was best modeled by an elastic plate considerably thicker than the plate which best fit the bathymetry as determined in other studies, many of which are listed in Table 5. Because most studies of elastic thickness are performed using bathymetric data, we will primarily discuss the results we obtained using this type of data.

Inelastic Processes

The above discussion of T_e from the Peru Trench in terms of the depth to the isotherm at the elastic/ductile transition is predicated on the assumption that there is no inelastic yielding. However, the fact that the elastic plate thickness at North Chile is smaller (22 vs. 28 km) in spite of the greater lithospheric age suggests that inelastic yielding might be a factor, at least for North Chile if not for Peru. Apparently, at high plate curvature ($K > 10^{-6}$ m^{-1}), the reduction in elastic plate thickness from such yielding can more than offset the expected increase in plate thickness over 15 m.y. of thermal cooling. If we assume that the plate near the Peru trench is undergoing little failure, then the 700°C isotherm can be taken to be the base of the mechanical plate. This isotherm should fall near

a depth of 34 km in 45 Ma lithosphere. The observed elastic thickness of 22 km then implies that the plate is failing through a total of 12 km, or 35% of its thickness.

McNutt [1984] has calculated the expected reduction in observed elastic plate thickness as curvature of the plate increases for a rheological model similar to that shown in Figure 1b. The results of that study can be applied to our results, both as a test of the practical application of those calculations and as confirmation (or denial) of the degree of yielding we have deduced for the plate at the North Chile Trench. The conversion from T_e, the effective elastic thickness, to T_m, the mechanical thickness which marks the true depth to the elastic/ductile transition, is somewhat dependent on in-plane stresses P. For a T_e-value of 28 km and a plate curvature of 3×10^{-7} m^{-1} (Peru), the value for T_m, which equals T_e only in the limit of no plate curvature, is expected to be 32 km [*McNutt*, 1984, Figure 3]. A regional tensional stress of as much as 100 MPa, probably unlikely in a convergence zone without backarc opening, would increase T_m by 2 km, and a regional compression of similar magnitude would reduce it by 1 km. For the North Chile Trench, an elastic thickness of 22 km with a plate curvature of 13×10^{-7} m^{-1} should have a mechanical thickness of 38 km. For both trenches, the implied mechanical thickness of the lithosphere implies an isotherm at the base of the plate between 764°C and 783°C. These values are extremely close to the temperature of 800°C predicted for the elastic/ductile transition by simply extrapolating laboratory-derived flow laws to geologic strain rates [*Kirby*, 1980]. Studies of the focal depths of intraplate earthquakes [*Wiens and Stein*, 1983] also conclude that the elastic/ductile transition is marked by the 800°C isotherm.

In order to interpret the results of this study in support of temperatures less than 500°C at T_m, one would have to ignore the Peru Trench completely and discount inelastic yielding for North Chile. However, geologic evidence of faulting in and near the trench also supports the existence of yielding due to the curvature of the plate. Faulting on the outer trench wall is not well resolved on the 5-minute grid of the data used in this study, but is apparent in profiles taken along ship tracks across the Peru-Chile Trench [*Fisher and Raitt*,

1962; *Schweller et al.*, 1981]. These show numerous step faults and some graben structures. Step faults exist along the entire trench, with their average offset several hundred meters except in the North Chile region, where offsets of a kilometer exist [*Schweller et al.*, 1981]. Grabens appear primarily in the North Chile region. Evidence suggests that these features extend to depths of 4 to 7 km [*Schweller et al.*, 1981]. They reflect the failure that exists in the extensional, brittle upper zone of the plate. If this failure is the result of curvature-induced brittle failure, then it also suggests the presence of a somewhat lesser amount of yielding at the base of the plate, although accomplished through different mechanisms (Figure 1b).

Correlation between Plate Dip and Elastic Thickness

Although a relationship between plate dip and the downward curvature of a plate is appealing, and the evidence from the Peru-Chile appears to support such a relationship, a further look at the region indicates that plate dip may not explain the variation in curvature, and therefore elastic thickness. The slope of the slab beneath Peru averages 15°, while beneath northern Chile it descends at approximately 33° [*Barazangi and Isacks*, 1976; *Barazangi and Isacks*, 1979a]. However, detailed analysis of the trends of the hypocentral surfaces indicates that in the upper 100 km the plate descends at the same slope in both regions, and then flattens under Peru while continuing to descend under northern Chile [*Bevis and Isacks*, 1984; *Chowdhury and Whiteman*, 1987]. Also, while the deep dip of the plate is greater in this region than it is to the north, it is not great compared to the plate dip in other subduction zones throughout the world [*Isacks and Barazangi*, 1977], and therefore would not be expected to be associated with such extreme downward curvature of the plate as compared to those at subduction zones elsewhere in the world [*McNutt and Menard*, 1982].

Such worldwide elastic thickness and plate dip data is shown in Table 5. The values of elastic thickness are those determined in studies of elastic and elastic-plastic behavior, and

the angle of dip is obtained from published cross-sections showing the locations of earthquake hypocenters,. Also listed in Table 5 are approximate elastic thicknesses at 100 Ma, calculated assuming that T_e remains proportional to the depth of the 800° isotherm of a 125-km-thick thermal plate [*Parsons and Sclater*, 1977]. These elastic thickness data, averaged over regions of constant dip within each trench, are plotted in Figure 12. No relationship between the two parameters is apparent in the plots. The dip of the plate in most of the subduction zones for which these data exist falls within a relatively small range between 40° and 65°, and although the dip of the earthquake hypocenters in each published study could be determined to within a few degrees, the dip of the same portion of the plate varied by up to 10° between studies. Though it seems highly unlikely from this study, it is possible that uncertainties in the data mask a trend.

The relationship between plate dip and T_e investigated here was presumed to occur, if it did, due to the increased curvature of the plate entering a more steeply dipping subduction zone. In order to investigate whether the dip of the plate at such depths does affect the curvature of the plate, curvature at the first zero crossing is plotted against plate dip in Figure 13. The curvature is obtained from values for the height and position of the outer rise published in the studies from which elastic thickness was obtained (Table 5). This data appears similar to the T_e-dip data. These plots give no support for a relationship between plate dip at depth and the elastic characteristics of that plate at the surface.

Correlation between Trench Curvature and Elastic Plate Thickness

McNutt et al. [1988] have found that the maximum elastic thickness of the plate at a continental convergence zone appears to bear an inverse relationship to the radius of curvature of the thrust belt in map view. This relationship was first investigated in an earlier study [*McNutt and Kogan*, 1986] because an application of the geometry of an inextensible, flexible, spherical shell suggests that the curvature of a trench as seen in map view is linearly related to the dip of the subducted slab [*Frank*, 1968]. In continental zones,

where little data is available concerning the dip of the plate, this curvature might then provide a means of understanding the condition of the plate at depth. As such, it was expected that when the plate dipped steeply, the elastic thickness would be small. However, the geometrical argument suggests that as plate dip increases, and elastic thickness decreases, the radius of curvature also increases, while *McNutt and Kogan* [1986] and *McNutt et al.* [1988] found that as radius of curvature increases the maximum observed elastic thickness becomes larger.

Further studies [*Laravie*, 1975; *Tovish and Schubert*, 1978] have produced no evidence for a relationship between plate dip and areal curvature of the subduction zone, and the plate dip data compiled in the previous section of this study does not appear to show any correlation with the surface curvature of the associated trenches (Table 6). However, the models presented by *Strobach* [1973] and *Bayly* [1982] have suggested that the areal curvature of the trench may be more closely related to the dip of the plate near the surface than to its dip below 100 km, where it may be deformed by stresses. In view of these studies and the apparently contradictory relationship observed by *McNutt et al.* [1988], the elastic thicknesses from Table 5 were plotted against the radii of curvature found by *Tovish and Schubert* [1978] for the volcanic fronts of the accompanying volcanic arcs. In Figure 14a, the elastic thickness with no adjustment for age correction is shown. The maximum value of the elastic thickness does appear to increase as the radius of curvature of the trench increases, although the effect is not as marked as it is in the continental data of *McNutt et al.* [1988]. Their elastic thickness data is also not adjusted for the age of the plates involved, but most were of similar age. When such an adjustment is applied to the data in this study (Figure 14b), no trend is apparent. Any relationship between elastic thickness and arc curvature must be the result of the strength of the plate, regardless of its age. These results are consistent with the argument made by *McNutt et al.* [1988], that a strong plate will produce a straight front, while a weak plate may result in either a straight or curved front, dependent on the geometry of the subduction zone.

CONCLUSIONS

This investigation of the elastic thickness and curvature of the lithosphere entering the Peru-Chile trench confirms the existence of a major change in many characteristics of the trench between the region lying off the coast of northern Peru from 6°S to 15°S and the region off the coast of northern Chile between 17°S and 20°S. In this interval large changes occur in elastic thickness, downward curvature of the plate, and dip of the plate under South America. The 30-My-old plate off Peru has an elastic thickness of 28±4 km and a curvature of $(2.8\pm0.4)\times10^{-7}$ m^{-1}, and dips at 15°, while the 45-My-old plate off northern Chile has an elastic thickness of 22±2 km, a curvature of $(13.\pm2.)\times10^{-7}$ m^{-1}, and dips at 33°. The older yet thinner plate of northern Chile indicates that the stresses induced by the curvature there are causing the plate to yield to a greater extent than occurs off Peru, where the smaller curvature induces correspondingly smaller stresses and less yielding. The presence of this failure in the plate is supported by the faulting observed on the outer trench wall, which is much more extensive in the sharply bent plate off Chile. It does not appear that the extreme downward curvature at the Chile Trench is related to the change in the dip of the plate at depth, a result supported by a review of worldwide subduction zone data. On the other hand, the sharp areal curvature of the trench off the coast of northern Chile may be related to the relative weakness of the plate there.

The temperature at a depth corresponding to the effective elastic plate thickness of the North Chile Trench, 473±40°C, is similar to estimates of the temperature at the base of the plate derived from observations of elastic plate thickness beneath midplate volcanos [*Watts et al.*, 1980; *Calmant and Cazenave*, 1988]. However, our results indicate that the isotherm defining the base of the mechanical lithosphere must be at least 700°C to be consistent with the elastic thickness observed near the Peru Trench. This implies that the plate entering the North Chile Trench must be yielding to such an extent that the effective elastic thickness is approximately 65% of the plate's mechanical thickness. If theoretical calculations of the

relationship between mechanical and elastic thickness are used, we conclude that T_e may be as little as 58% of T_m, and the base of the mechanical plate is defined by an isotherm between 764°C and 783°C. Either result leads to the conclusion that the temperature at the base of the mechanical plate must be considerably above 500°C. In order to reconcile this with the results of lithospheric studies at midplate volcanoes, where stresses are lower and such yielding should not occur, we believe that the geotherm must be significantly disturbed under these features.

REFERENCES

Barazangi, M., and B.L. Isacks, Spatial distribution of earthquakes and subduction of the Nazca plate beneath South America, *Geology*, **4**, 686–692, 1976.

Barazangi, M., and B.L. Isacks, Subduction of the Nazca plate beneath Peru: evidence from spatial distribution of earthquakes, *Geophys. J. R. Astr. Soc.*, **57**, 537–555, 1979a.

Barazangi, M., and B.L. Isacks, A comparison of the spatial distribution of mantle earthquakes determined from data produced by local and by teleseismic networks for the Japan and Aleutian arcs, *Seism. Soc. Amer. Bull.*, **69**, 1763–1770, 1979b.

Bayly, B., Geometry of subducted plates and island arcs viewed as a buckling problem, *Geology*, **10**, 629–632, 1982.

Bevis, M., and B.L. Isacks, Hypocentral trend surface analysis: Probing the geometry of Benioff zones, *J. Geophys. Res.*, **89**, 6153–6170, 1984.

Bodine, J.H., and A.B. Watts, On lithospheric flexure seaward of the Bonin and Mariana trenches, *Earth Plan. Sci. Lett.*, **43**, 132–148, 1979.

Brace, W.F., and D.L. Kohlstedt, Limits on lithospheric stress imposed by laboratory experiments, J. Geophys. Res., **85**, 6248–6252, 1980.

Brotchie, J.F., Flexure of a liquid-filled spherical shell in a radial gravity field, *Modern Geology*, **3**, 15–23, 1971.

Burbach, G.V.N., C. Frolich, W.D. Pennington, and T. Matumoto, Seismicity and tectonics of the subducted Cocos plate, *J. Geophys. Res.*, **89**, 7719–7735, 1984.

Caldwell, J.G., W.F. Haxby, D.E. Karig, and D.L. Turcotte, On the applicability of a universal elastic trench profile, *Earth Plan. Sci. Lett.*, **31**, 239–246, 1976.

Cardwell, R.K., B.L. Isacks, and D.E. Karig, The spatial distribution of earthquakes, focal mechanism solutions, and subducted lithosphere in the Philippine and northeastern Indonesian islands, in *The Tectonic and Geologic Evolution of Southeast Asian Seas and Islands*, Geophys. Monogr. Ser., vol. **23**, edited by D.E. Hayes, pp 177–202, AGU, Washington, D.C., 1980.

Carey, E., and J. Dubois, Behavior of the oceanic lithosphere at subduction zones; plastic yield strength from a finite-element method, *Tectonophysics*, **74**, 99–110, 1981.

Carr, M.J., Underthrusting and Quaternary faulting in northern Central America, *Geol. Soc. Amer. Bull.*, **87**, 825–829, 1976.

Carr, M.J., R.E. Stoiber, and C.L. Drake, Discontinuities in the deep seismic zones under the Japanese arcs, *Geol. Soc. Amer. Bull.*, **84**, 2917–2930, 1973.

Chowdhury, D.K., and S.K. Whiteman, Structure of the Benioff zone under Southern Peru to Central Chile, *Tectonophysics*, **134**, 215–226, 1987.

Coudert, E., B.L. Isacks, M. Barazangi, R. Louat, R. Cardwell, A. Chen, J. Dubois, G. Latham, and B. Pontoise, Spatial distribution and mechanisms of earthquakes in the southern New Hebrides arc from a temporary land and ocean bottom seismic network and from worldwide observations, *J. Geophys. Res.*, **86**, 5905–5925, 1981.

Dang, S., Seismic refraction velocity structure, Sheet 9, in *Peru-Chile Trench Off Peru*, Ocean Margin Drilling Program, Regional Atlas Series, Atlas **9**, edited by D.M. Hussong, S.P. Dang, L.D. Kulm, R.W. Couch, and T.W.C. Hilde, Marine Science International, Woods Hole, Mass., 1984.

Dewey, J. W., and S.T. Algermissen, Seismicity of the Middle America arc-trench system near Managua, Nicaragua, *Seism. Soc. Amer. Bull.*, **64**, 1033–1048, 1974.

Dubois, J., Propagation of P waves and Rayleigh Waves in Melanesia: Structural implications, *J. Geophys. Res.*, **76**, 7217–7240, 1971.

Engdahl, E.R., Seismicity of plate subduction in the Central Aleutians, in *Island Arcs, Deep Sea Trenches, and Back Arc Basins*, Maurice Ewing Ser., vol. **1**, edited by M. Talwani and W.C. Pitman, pp 259–271, AGU, Washington, D.C., 1977.

Erlandson, D.L., D.M. Hussong, and J.F. Campbell, Sediment and associated structure of the northern Nazca plate, in *Nazca Plate: Crustal Formation and Andean Convergence*, edited by L.D. Kulm, J. Dymond, E.J. Dasch, and D.M. Hussong, *Geol. Soc. Amer. Mem.*, **154**, pp 295–314, 1981.

Fisher, R.L., and R.W. Raitt, Topography and structure of the Peru-Chile trench, *Deep-Sea Res.*, **9**, 423–443, 1962.

Fitch, T.J., and P. Molnar, Focal mechanisms along inclined earthquake zones in the Indonesia-Philippine region, *J. Geophys. Res*, **75**, 1431–1444, 1970.

Frank, F.C., Curvature of island arcs, *Nature*, **220**, 363, 1968.

Frohlich, C., S. Billington, E.R. Engdahl, and A. Malahoff, Detection and location of earthquakes in the Central Aleutian subduction zone using island and ocean bottom seismograph stations, *J. Geophys. Res.*, **87**, 6853–6864, 1982.

Goetze, C., and B. Evans, Stress and temperature in the bending lithosphere as constrained by experimental rock mechanics, *Geophys. J. R. Astr. Soc.*, **59**, 463–478, 1979.

Handschumacher, D.W., Post-Eocene plate tectonics of the eastern Pacific, in *The Geophysics of the Pacific Ocean Basin and its Margin*, Geophys. Monogr. Ser., vol. **19**, edited by G.H. Sutton, M.H. Manghnani, and R. Moberly, pp 177–202, AGU, Washington, D.C., 1976.

Heirtzler, J.R., and M. Edwards, Relief of the surface of the Earth, Report MGG-2, National Geophysical Data Center, Boulder, Colo., 1985.

Herron, E.M., Sea-floor spreading and the Cenozoic history of the East Central Pacific, *Geol. Soc. Amer. Bull.*, **83**, 1671–1692, 1972.

Hilde, T.W.C., and W.E.K. Warsi, Magnetic anomaly profiles, Sheet 4, in *Peru-Chile Trench Off Peru*, Ocean Margin Drilling Program, Regional Atlas Series, Atlas **9**,

edited by D.M. Hussong, S.P. Dang, L.D. Kulm, R.W. Couch, and T.W.C. Hilde, Marine Science International, Woods Hole, Mass., 1984.

Hussong, D.M., P.B. Edwards, S.H. Johnson, J.F. Campbell, and G.H. Sutton, Crustal structure of the Peru-Chile Trench: 8°–12° S latitude, in *The Geophysics of the Pacific Ocean Basin and its Margin*, Geophys. Monogr. Ser., vol. **19**, edited by G.H. Sutton, M.H. Manghnani, and R. Moberly, pp 71-85, AGU, Washington, D.C., 1976.

Isacks, B.L., and M. Barazangi, Geometry of Benioff Zones: Lateral segmentation and downwards bending of the subducted lithosphere, in *Island Arcs, Deep Sea Trenches, and Back Arc Basins*, Maurice Ewing Ser., vol. **1**, edited by M. Talwani and W.C. Pitman, pp 99–114, AGU, Washington, D.C., 1977.

Jones, G.M., T.W.C. Hilde, G.F. Sharman, and D.C. Agnew, Fault patterns in outer trench walls and their tectonic significance, *J. Phys. Earth*, **26**, Suppl., S 85–S 101, 1978.

Laravie, J.A., Geometry and lateral strain of subducted plates in island arcs, *Geology*, **3**, 484–486, 1975.

Katsumata, M., and L.R. Sykes, Seismicity and tectonics of the western Pacific: Izu-Mariana-Caroline and Ryukyu-Taiwan Regions, *J. Geophys. Res.*, **74**, 5923–5948, 1969.

Kirby, S.H., Tectonic strresses in the lithosphere: Constraints provided by the experimental deformation of rocks, *J. Geophys. Res.*, **85**, 6353–6363, 1980.

Marsh, J.G., A.C. Brenner, B.D. Beckley, and T.V. Martin, Global mean sea surface based upon the Seasat altimeter data, *J. Geophys. Res.*, **91**, 3501–3506, 1986.

McAdoo, D.C., and C.F. Martin, Seasat observations of lithospheric flexure seaward of trenches, *J. Geophys. Res.*, **89**, 3201–3210, 1984.

McAdoo, D.C., and D.T. Sandwell, Folding of oceanic lithosphere, *J. Geophys. Res.*, **90**, 8563–8569, 1985.

McAdoo, D.C., J.G. Caldwell, and D.L. Turcotte, On the elastic-perfectly plastic bending of the lithosphere under generalized loading with application to the Kuril Trench, *Geophys. J. R. Astr. Soc.*, **54**, 11–26, 1978.

McAdoo, D.C., C.F. Martin, and S. Poulose, Seasat observations of flexure: evidence for a strong lithosphere, *Tectonophysics*, **116**, 209–222, 1985.

McNutt, M.K., Lithospheric flexure and thermal anomalies, *J. Geophys. Res.*, **89**, 11,180–11,194, 1984.

McNutt, M.K., and H.W. Menard, Constraints on yield strength in the oceanic lithosphere derived from observations of flexure, *Geophys. J. R. Astr. Soc.*, **71**, 363–394, 1982.

McNutt, M.K, and M.G. Kogan, Isostasy in the USSR II: Interpretation of admittance data, in *The Composition, Structure, and Dynamics of the Lithosphere-Asthenosphere System*, Geodynamic Ser., edited by K. Fuchs and C. Froidevaux, AGU, Washington, D.C., 1986.

McNutt, M.K., M. Diament, and M.G. Kogan, Variations of elastic plate thickness at continental thrust belts, *J. Geophys. Res.*, in press

Mitronovas, W., and B. Isacks, Seismic velocity anomalies in the upper mantle beneath the Tonga-Kermadec island arc, *J. Geophys. Res.*, **76**, 7154–7180, 1971.

Mitronovas, W., B. Isacks, and L. Seeber, Earthquake locations and seismic wave propagation in the upper 250 km of the Tonga island arc, *Seism. Soc. Amer. Bull.*, **59**, 1115–1135, 1969.

Parsons, B.E., and J. Sclater, An analysis of the variation of ocean floor bathymetry and heat flow with age, *J. Geophys. Res.*, **82**, 803–827, 1977.

Pascal, G., B.L. Isacks, M. Barazangi, and J. Dubois, Precise relocations of earthquakes and seismotectonics of the New Hebrides island arc, *J. Geophys. Res.*, **83**, 4957–4973.

Scheidegger, K.F., and J.B. Corliss, Petrogenesis and secondary alteration of upper layer 2 basalts of the Nazca plate, in *Nazca Plate: Crustal Formation and Andean Convergence*, edited by L.D. Kulm, J. Dymond, E.J. Dasch, and D.M. Hussong, *Geol. Soc. Amer. Mem.*, **154**, pp 77–107, 1981.

Schweller, W.J., L.D. Kulm, and R.A. Prince, Tectonics, structure, and sedimentary framework of the Peru-Chile Trench, in *Nazca Plate: Crustal Formation and Andean Convergence*, edited by L.D. Kulm, J. Dymond, E.J. Dasch, and D.M. Hussong, *Geol. Soc. Amer. Mem.*, **154**, pp 323–349, 1981.

Strobach, K., Curvature of island arcs and plate tectonics, *Zeitschrift für Geophysik*, **39**, 819–831, 1973.

Sykes, L.R, The seismicity and deep structure of island arcs, *J. Geophys. Res.*, **71**, 2981–3006, 1966.

Sykes, L.R., and M. Ewing, The seismicity of the Caribbean region, *J. Geophys. Res.*, **70**, 5065–5074, 1965.

Sykes, L.R., B.L. Isacks, and J. Oliver, Spatial distribution of deep and shallow earthquakes of small magnitude in the Fiji-Tonga region, *Seism. Soc. Amer. Bull.*, **59**, 1093–1113, 1969.

Tovish, A., and G. Schubert, Island arc curvature, velocity of convergence, and angle of subduction, *Geophys. Res. Lett.*, **5**, 329–332, 1978.

Turcotte, D.L,and G. Schubert, *Geodynamics: Applications of Continuum Physics to Geological Problems*, John Wiley and Sons, N.Y., 1982.

Turcotte, D.L, D.C. McAdoo, and J.G. Caldwell, An elastic-perfectly plastic analysis of the bending of the lithosphere at a trench, *Tectonophysics*, **47**, 193–205, 1978.

Wiens,D.A, and S. Stein, Age dependence of oceanic intraplate seismicity and implications for lithospheric evolution, *J. Geophys. Res.*, **88**, 6455–6468, 1983.

Westbrook, G.K., The structure of the crust and upper mantle in the region of Barbados and the Lesser Antilles, *Geophys. J. R. Astr. Soc.*, **43**, 201–242, 1975.

Table 1: Elastic plate parameters at the Peru Trench from bathymetry

Profile No.	T_e (km)	M_o ($\times 10^{16}$ N)	V_o ($\times 10^{12}$ Nm^{-1})	K(0) ($\times 10^{-7}$ m^{-1})	misfit (m)	half-width (km)
NORTHERN PERU						
1	30.3	7.4	0.21	2.45	30.0	9.4
2	26.7	4.9	0.43	2.51	19.7	5.7
3	23.4	3.1	0.47	2.47	15.0	4.5
4	20.6	1.5	0.60	2.35	18.2	6.2
5	17.0	-4.2	0.79	2.30	17.8	6.1
11	24.6	4.4	0.38	2.86	23.1	6.9
12	27.3	6.7	0.17	2.99	22.6	6.3
13	29.1	8.2	0.04	3.02	23.6	6.2
14	31.6	10.3	-0.11	2.96	29.6	8
15	32.5	11.4	-0.25	3.02	31.4	8
16	32.0	11.5	-0.26	3.22	27.0	7.1
17	30.9	10.8	-0.15	3.31	21.8	5.3
18	29.4	9.6	-0.22	3.47	27.5	6.5
19	29.4	8.5	0.12	3.06	23.1	6.0
20	28.8	7.1	0.37	2.79	19.9	5.7
21	29.4	5.6	0.56	2.19	22.6	8.3
SOUTHERN PERU						
6	7.1			2.90	9.3	4
7	8.9			2.33	4.2	2.1
8	9.7			2.18	5.2	2.7
9	10.2			2.28	4.6	2.2
10	10.2			2.52	4.9	2.0
11	10.4			2.67	3.6	1.4
12	10.8			3.02	4.7	1.6

Table 2: Elastic plate parameters at the Peru Trench from geoid height

Profile No.	T_e (km)	M_o ($\times 10^{16}$ N)	V_o ($\times 10^{12}$ Nm^{-1})	K(0) ($\times 10^{-7}$ m^{-1})	misfit (m)	half-width (km)
NORTHERN PERU						
10	31.0	6.08	0.21	1.88	0.101	7.4
13	35.2	8.00	0.12	1.67	0.088	6.8
16	34.1	7.55	0.11	1.73	0.089	6.7
19	35.4	8.46	0.07	1.73	0.108	8.5
22	36.3	8.80	0.14	1.68	0.094	7.1
25	34.6	7.99	0.26	1.77	0.085	5.9
28	34.4	7.73	0.20	1.74	0.075	5.2
31	36.2	7.75	0.25	1.50	0.085	6.7
SOUTHERN PERU						
1	38.6	8.73	0.14	1.39	0.052	4.9
10	37.3	7.66	0.32	1.37	0.065	5.9
13	39.4	8.28	0.30	1.26	0.055	5.4
16	38.3	8.74	0.20	1.42	0.049	4.2
19	37.6	9.93	0.15	1.70	0.075	5.7
22	39.3	11.1	0.09	1.66	0.055	4.1
25	38.5	10.4	0.07	1.65	0.051	3.8
28	39.0	10.6	0.05	1.62	0.059	4.4
31	41.5	12.6	-0.09	1.59	0.049	3.8
34	41.8	13.9	-0.16	1.72	0.051	3.8
37	42.1	13.8	-0.29	1.70	0.043	3.3
40	41.4	12.4	-0.11	1.58	0.070	6.1
43	39.7	11.2	-0.14	1.63	0.065	5.5
46	36.3	9.00	-0.30	1.75	0.042	3.8
49	35.6	9.43	-0.38	1.97	0.061	4.3
52	37.1	10.4	-0.47	1.96	0.064	4.8
55	38.7	10.6	-0.33	1.70	0.046	3.9
58	41.7	10.5	-0.37	1.37	0.043	4.6

Table 3: Elastic plate parameters at the North Chile Trench from bathymetry

Profile No.	T_e (km)	M_o (x1016 N)	V_o (x1012 Nm-1)	K(0) (x10-7 m-1)	misfit (m)	half-width (km)
REGION 1						
13	24.5	7.9	0.30	4.91	52.5	10.0
14	21.9	6.7	0.27	5.86	55.4	8.3
24	19.8	10.2	-0.40	12.2	86.4	8.3
25	22.9	14.0	-0.83	11.1	96.1	8.4
26	22.8	14.6	-0.92	11.7	91.6	7.9
27	21.5	13.2	-0.90	12.7	83.5	7.1
28	19.8	11.1	-0.81	13.7	88.9	7.7
35	21.2	13.7	-1.18	14.3	88.0	7.9
36	22.4	14.9	-1.03	12.8	67.1	6.3
37	24.5	16.0	-1.05	10.5	62.9	5.8
38	24.2	15.1	-1.02	10.2	46.6	4.4
39	23.3	14.4	-0.97	11.0	49.7	4.4
40	21.9	13.6	-1.03	12.5	72.2	5.7
41	21.9	13.3	-0.86	12.0	73.9	5.6
42	22.4	13.7	-0.80	11.5	74.5	5.7
REGION 2						
1	22.6	15.8	-1.26	13.5	51.6	4.1
2	22.7	15.5	-1.23	13.1	52.4	4.2
3	22.4	14.9	-1.08	12.8	65.4	5.1
4	21.5	13.8	-0.94	13.2	67.6	5.0
5	20.9	13.2	-0.88	13.8	65.1	4.7
6	20.9	13.2	-0.84	14.0	72.6	5.2
7	20.4	12.8	-0.78	14.3	83.0	5.8
REGION 3						
1	22.9	16.5	-0.86	12.9	91.1	6.6
REGION 5						
1	17.8	10.5	-0.58	17.4	91.0	5.8
2	17.2	8.6	-0.39	15.6	74.6	5.3
6	17.8	8.6	-0.22	14.0	77.5	4.9
7	17.8	8.6	-0.27	14.0	75.0	4.9

Table 4: Elastic plate parameters at the North Chile Trench from geoid height

Profile No.	T_e (km)	M_o (x1016 N)	V_o (x1012 Nm-1)	K(0) (x10-7 m-1)	misfit (m)	half-width (km)
REGION 1						
10	34.0	11.2	0.03	2.57	0.129	8.6
13	35.7	13.3	-0.05	2.66	0.136	8.0
25	28.0	9.27	0.11	3.84	0.151	7.6
28	26.3	9.52	-0.23	4.76	0.152	6.6
31	23.2	8.80	-0.40	6.5	0.142	5.3
34	24.6	10.1	-0.43	6.3	0.162	6.2
37	25.6	12.1	-0.59	6.8	0.161	5.0
REGION 2						
1	21.5	8.48	-0.37	7.9	0.101	3.5
4	22.1	9.39	-0.51	8.1	0.142	5.2
7	23.7	10.9	-0.43	7.5	0.165	5.8
REGION 3						
1	23.2	10.9	-0.32	7.9	0.132	4.0
4	24.0	12.2	-0.31	8.0	0.159	4.4
REGION 4						
1	23.6	11.8	-0.33	8.2	0.154	4.3
REGION 5						
1	23.0	8.73	-0.01	6.5	0.160	5.5
4	26.3	9.24	0.10	4.59	0.114	4.7
31	29.0	11.6	0.64	4.48	0.136	4.1
34	27.6	11.0	0.66	4.91	0.118	3.5
37	26.9	10.3	0.65	4.97	0.131	4.1

Table 5: Elastic thickness and dip of the plate at subduction zones. T_e^c is the elastic thickness expected at 100 My. Errors are included when specified by the source.

Profile name	Age	T_e	T_e^c	dip	source (T_e)
Aleutian Seamap 13	55	26	35	63°	Caldwell *et al.*, 1976
Aleutian Seamap 13	55	25	33	63	Turcotte *et al.*, 1978
Aleutian Seamap 13-4	55	38±5	50	63	Jones *et al.*, 1978
Aleutian	55–70	34	45	63	Carey & Dubois, 1981
Kuril Zetes 2-1	100	17±6	17	53	Jones *et al.*, 1978
Kuril	100	19	19	47	Caldwell *et al.*, 1976
Kuril	100	29	29	47	Carey & Dubois, 1981
Kuril Zetes 2-6	100	22±3	22	44	Jones *et al.*, 1978
Bonin Hunt 1-4	130	32±5	29	50	Jones *et al.*, 1978
Bonin Bent 1-3	130	25±5	23	50	Jones *et al.*, 1978
Bonin Bent 2-2	130	29±4	26	50	Jones *et al.*, 1978
Bonin Aries 7/Hunt 3-2	130	28±4	25	55	Jones *et al.*, 1978
Bonin Aries 7/Hunt 3	130	26	24	55	Caldwell *et al.*, 1976
Mariana Scan 5	>165	27	23	80	Caldwell *et al.*, 1976
Mariana Scan 5	>165	22±5	19	80	Jones *et al.*, 1978
Mariana Scan 5	>165	29	25	80	Turcotte *et al.*, 1978
South Mariana	>165	32	27	80	Carey & Dubois, 1981
Manila Shelldrake	23	36±8	74	66	Jones *et al.*, 1978
Manila Maury	23	22±8	45	66	Jones *et al.*, 1978
Philippine (North)	50	43	60	60	Carey & Dubois, 1981
Philippine (South)	65	36	44	60	Carey & Dubois, 1981
New Hebrides	50	28	39	70	Carey & Dubois, 1981
Tonga Oceanographer	90	32	34	50	Turcotte *et al.*, 1978
Tonga (GEO 319, 321)	100	40	40	50	Carey & Dubois, 1981
Kermadec (GEO 316)	100	38	38	65	Carey & Dubois, 1981
Middle America Iguana 4-2	20	16±6	35	54	Jones *et al.*, 1978
Middle America Iguana 2	20	15±6	33	54	Jones *et al.*, 1978
Middle America	30–35	15	27	63	Carey & Dubois, 1981
Peru	30	30	54	15	Carey & Dubois, 1981
Peru	30	28±4	50	15	this study
Northern Chile	45	22±2	32	33	this study

Sources of plate dip data:

Aleutians: *Engdahl*, 1977; *Barazangi and Isacks*, 1979b; *Frohlich et al.*, 1982
Kurils: *Sykes*, 1966; *Isacks and Barazangi*, 1977
Bonin: *Carr et al.*, 1973; *Katsumata and Sykes*, 1969; *Isacks and Barazangi*, 1977
Marianas: *Katsumata and Sykes*, 1969; *Isacks and Barazangi*, 1977
Manila: *Cardwell et al.*, 1980
Philippines: *Cardwell et al.*, 1980
New Hebrides: *Dubois*, 1971; *Isacks and Barazangi*, 1977; *Pascal et al.*, 1979; *Coudert et al.*, 1981
Tonga: *Sykes*, 1966; *Sykes et al.*, 1969; *Mitronovas et al.*, 1969; *Mitronovas and Isacks*, 1971; *Isacks and Barazangi*, 1977
Kermadec: *Sykes*, 1966; *Isacks and Barazangi*, 1977
Middle America: *Dewey and Algermissen*, 1974; *Carr*, 1976; *Burbach et al.*, 1984
South America: *Barazangi and Isacks*, 1976; *Barazangi and Isacks*, 1979a

Table 6: Radius of curvature of trench in map view and dip of the plate.

Curvature	Location	Dip	Source for dip
0–10°			
	Lesser Antilles	47°	Westbrook, 1975
	Nicaragua	69°	Burbach *et al.*, 1984
	Northern Chile	30°	Isacks & Barazangi, 1977
	Marianas	80°	Isacks & Barazangi, 1977
	N. Japan (Honshu)	34°	Carr *et al.*, 1973
10–20°			
	Greater Antilles	53°	Sykes & Ewing, 1965
	Guatemala	63°	Burbach *et al.*, 1984
	Aleutians	61°	House & Boatwright, 1985
	Kamchatka	50–55°	Isacks & Barazangi, 1977
	Ryukyu	52°	Carr *et al.*, 1973
20–40°			
	Kuril	44–50°	Isacks & Barazangi, 1977
	Java	65°	Fitch & Molnar, 1970
	Philippine	70°	Fitch & Molnar, 1970
40–60°			
	Tonga	53°	Isacks & Barazangi, 1977
	Kermadec	70°	Isacks & Barazangi, 1977
60°+			
	Peru	15°	Isacks & Barazangi, 1977
	Central Chile	16°	Isacks & Barazangi, 1977
	Southern Chile	33°	Isacks & Barazangi, 1977
	Izu-Bonin	50–60°	Katsumata & Sykes, 1969

FIGURE CAPTIONS

Figure 1: (a) The distribution of stress difference ($\sigma_h - \sigma_v$) with depth in a downward bent perfectly elastic plate. Positive stress difference is extension; negative stress difference represents compression. The depth T_e represents the base of the elastic plate. (b) An approximation of the yield envelope for a rheological model of the lithosphere which includes brittle failure and sliding at shallow depths and failure by ductile creep in the lower plate. T_m is the base of the mechanical lithosphere. The inner line corresponding to the sloped line in (a) represents the stress difference due to curvature of such a plate, which experiences yielding near the surface and base. T_m will be greater than the measured T_e of such a plate. (Figure from *McNutt*, 1984)

Figure 2: (a) A plot of the minimum misfit at each value of elastic thickness for profile #3 in the northern region of the Peru province. The half-width is 4.5 km. (b) A similar plot for profile #5 in region 2 of the North Chile province. The half-width is 4.6 km.

Figure 3: (a) Location of the region studied. (b) Bathymetry of the region near the Peru Trench for which data were obtained, showing the location of the areas from which profiles were taken. (c) Bathymetry of the region near the northern Chile Trench for which data were obtained, showing the location of the areas from which profiles were taken.

Figure 4: A series of representative profiles across the Peru trench, extending 300 km to seaward and up to 70 km landward of the first zero crossing. NPER represents the northern region and SPER is the southern region. Those profiles which could be satisfactorily fit by the elastic model are shown with this model dashed in; those which could not are shown with a horizontal line at an estimated reference height.

Figure 5: The geoid along the same profiles for which bathymetry was shown in Figure 4. The solid line is the observed geoid, and the dashed line is the best-fitting theoretical geoid whcih could be generated from an elastic curve.

Figure 6: Observed bathymetry (solid line), the elastic curve which best fit the bathymetry (short-dashed line), and the elastic curve from which the geoid could best be modeled (long-dashed line) for profiles #16 of the northern region

Figure 7: A series of representative profiles across the northern part of the Chile trench, similar to those from the Peru trench in Figure 4. NCHIL1 is region 1, NCHIL2 is region 2, and NCHIL3 is region 3. Those profiles which could be satisfactorily fit by the elastic model are shown with this model dashed in; those which could not are shown with a horizontal line at an estimated reference height.

Figure 8: The geoid along the same profiles for which bathymetry was shown in Figure 7. The solid line is the observed geoid, and the dashed line is the best-fitting theoretical geoid generated from an elastic curve.

Figure 9: The observed geoid profile corresponding to bathymetric profile NCHIL2 #4 (solid line) and the result of modeling it from the bathymetry (dashed curve), rather than the elastic curve which was used to create the theoretical curve in Figure 8f.

Figure 10: Curves which result from modeling the bathymetry with an elastic plate of varying flexural rigidity. (a) The profile NPER #16 (solid line) shown with the curve

which results when the flexural rigidity changes from 25×10^{22} Nm (T_e=33 km) to 15×10^{22} Nm (T_e=28 km) (dashed line). The change occurs 50 km seaward of the zero-crossing, with the larger rigidity occurring to seaward. The theoretical curve obtained with a constant rigidity is shown in Figure 4d. (b) The profile NCHIL2 #4 (solid line) shown with the curve which results when the flexural rigidity changes from 35×10^{22} Nm (T_e=37 km) to 3.5×10^{22} Nm (T_e=17 km)(dashed line). The change occurs 55 km seaward of the zero-crossing. The curve resulting from an elastic model with constant rigidity is shown in Figure 8f. (c) Profile NCHIL2 #4 (solid line) shown with the curve which results when the flexural rigidity changes twice, from 35×10^{22} Nm (T_e=37 km) greater than 70 km seaward of the zero-crossing, to 2.5×10^{22} Nm (T_e=15 km) between 15 and 70 km seaward of the zero-crossing, to 15×10^{22} Nm (28 km) from x=15 km to the trench (dashed line).

Figure 11: Elastic curves resulting from a cylindrical load (short dashes) compared to that from a line load (long dashes) and the observed bathymetry (solid line) for profile NCHIL2 #4. The elastic curve produced by a line load uses the parameters which best fit the bathymetry (T_e=21.4 km), and is that shown in Figure 8f. (a) The curve produced by a cylindrical load acting on a plate with the same elastic thickness as that acted on by the line load. (b) The curve produced by a cylindrical load which best fit the bathymetry, found using an elastic thickness of 19.8 km.

Figure 12: (a) Plot of elastic thickness vs. plate dip using data from a number of studies. Elastic thicknesses are averaged over the values found, with the error bars representing the standard deviation. Points with no error bar were the only value found for that subduction zone and had no estimate of error. The data are in Table 5. (b) Similar plot but with elastic thicknesses estimated for a constant plate age of 100 My.

Figure 13: Plot of the curvature of the downward bent plate against the plate dip. Curvature was averaged over values obtained from measurements of the height and position of the outer rise published in the studies cited in Table 5.

Figure 14: (a) Elastic thickness, from same source as that in Figure 12, plotted against the radius of curvature of the volcanic arc associated with the subduction zone. Curvatures are from Tovish and Schubert (1978). (b) Similar plot with estimated elastic thickness at 100 My.

(a)

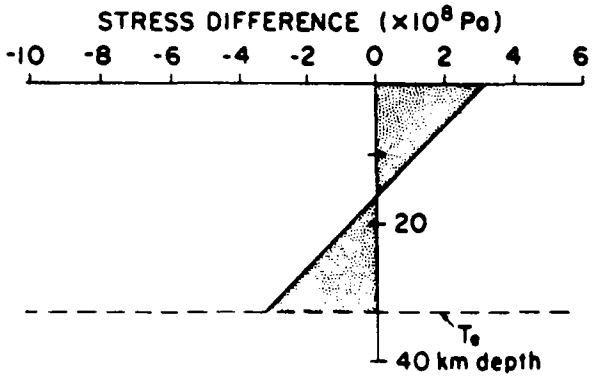
STRESS DIFFERENCE (×10⁸ Pa)
-10 -8 -6 -4 -2 0 2 4 6
20
Te
40 km depth

(b)

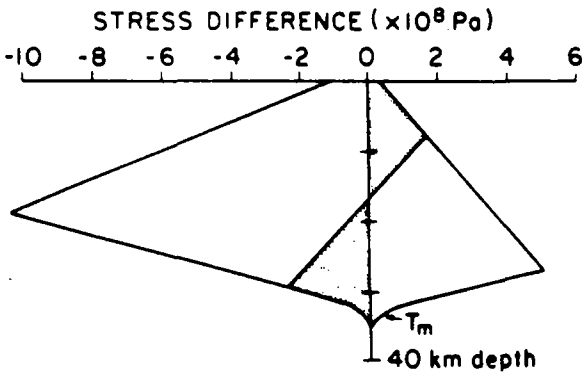
STRESS DIFFERENCE (×10⁸ Pa)
-10 -8 -6 -4 -2 0 2 4 6
Tm
40 km depth

figure 1

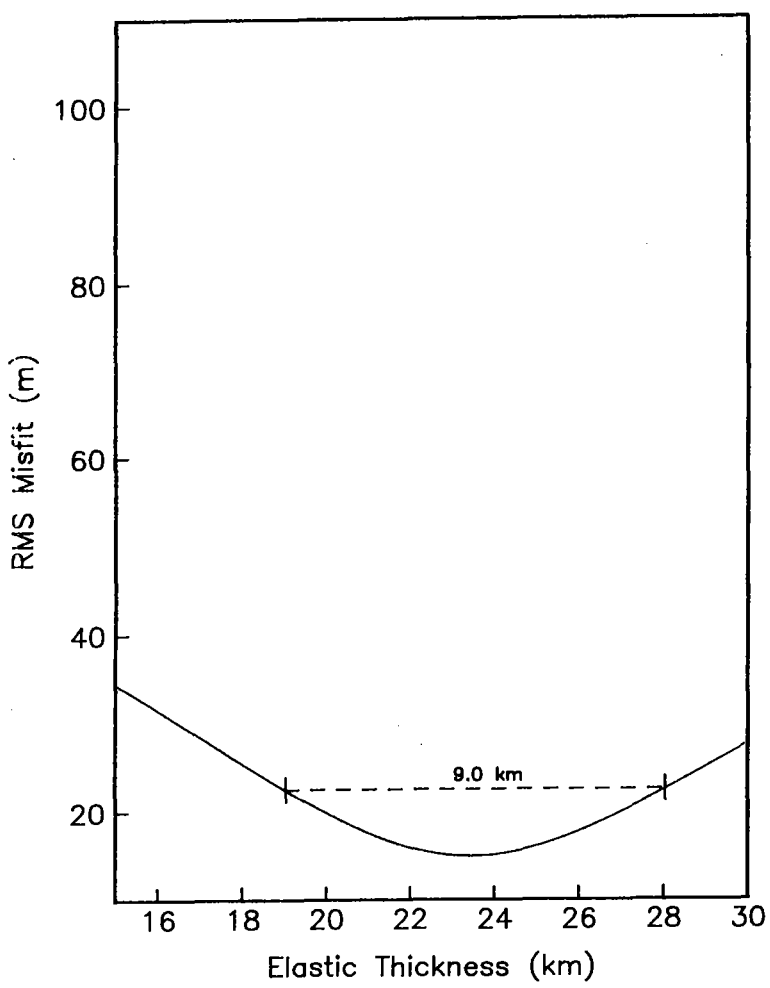
RMS Misfit (m)
100
80
60
40
20
9.0 km
16
18
20
22
24
26
28
30
Elastic Thickness (km)
(a)

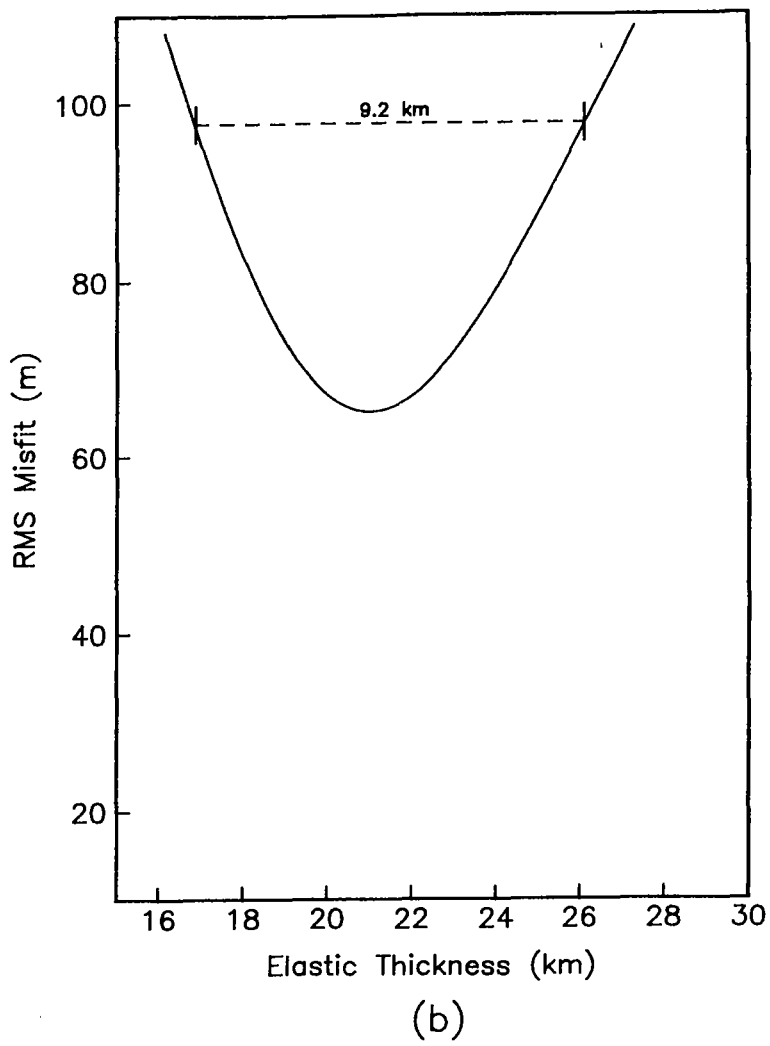
RMS Misfit (m)
100
80
60
40
20
9.2 km
16
18
20
22
24
26
28
30
Elastic Thickness (km)
(b)

Figure 2

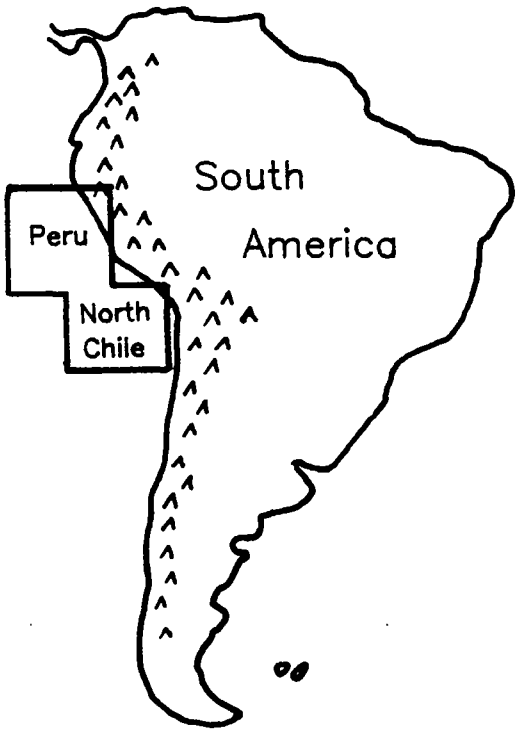

Figure 3 (a)

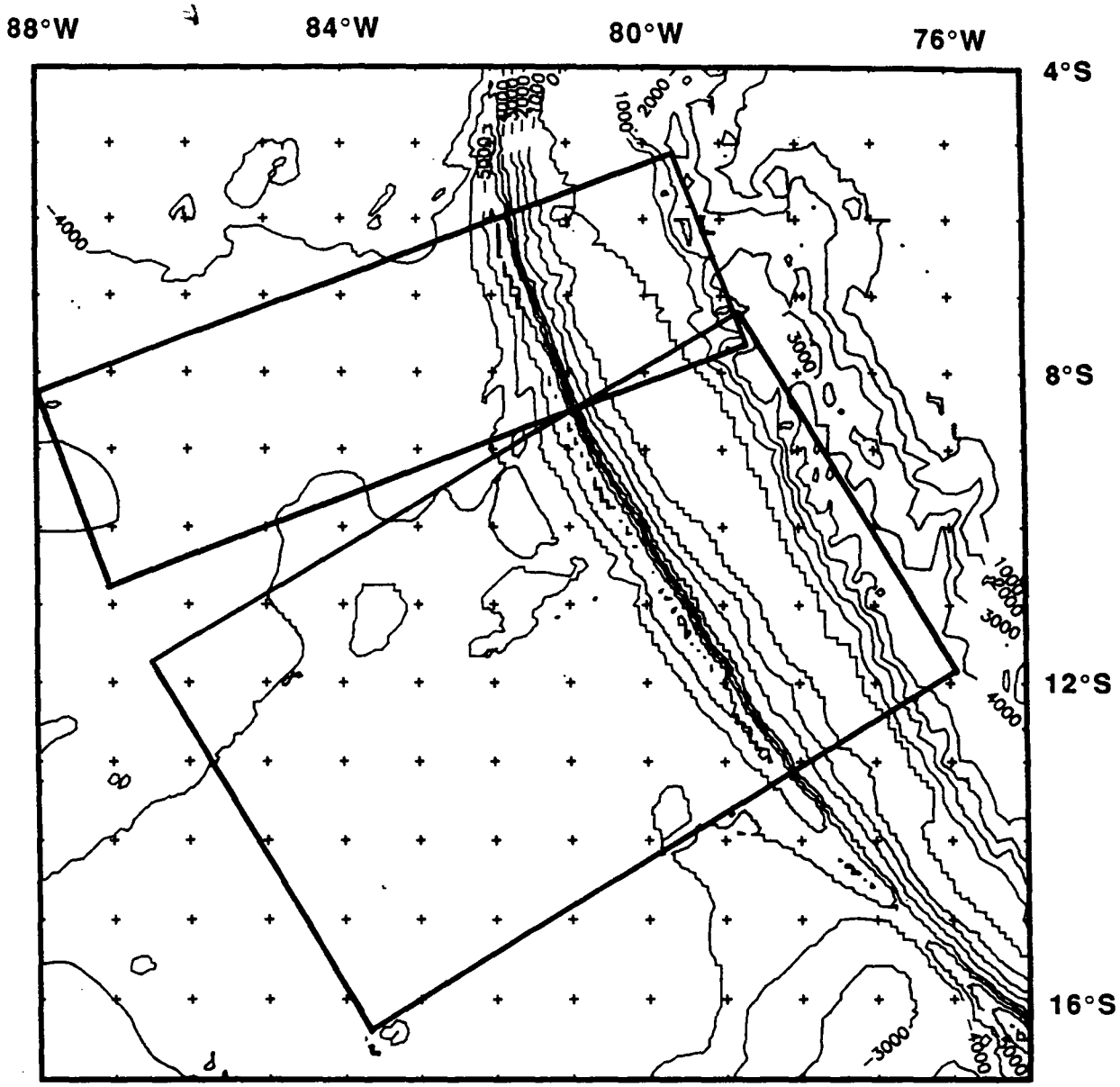

Figure 3 (b)

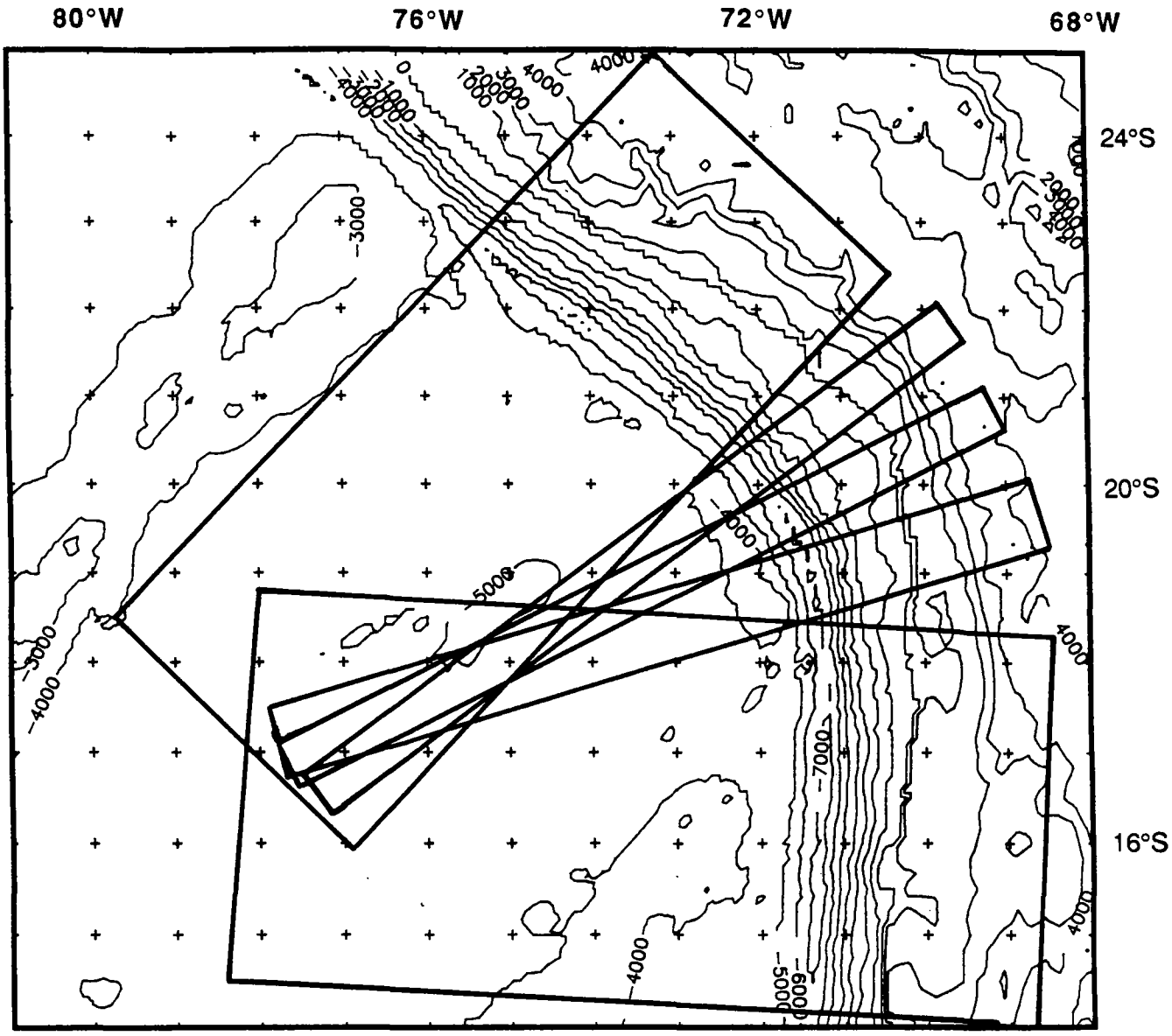

Figure 3 (c)

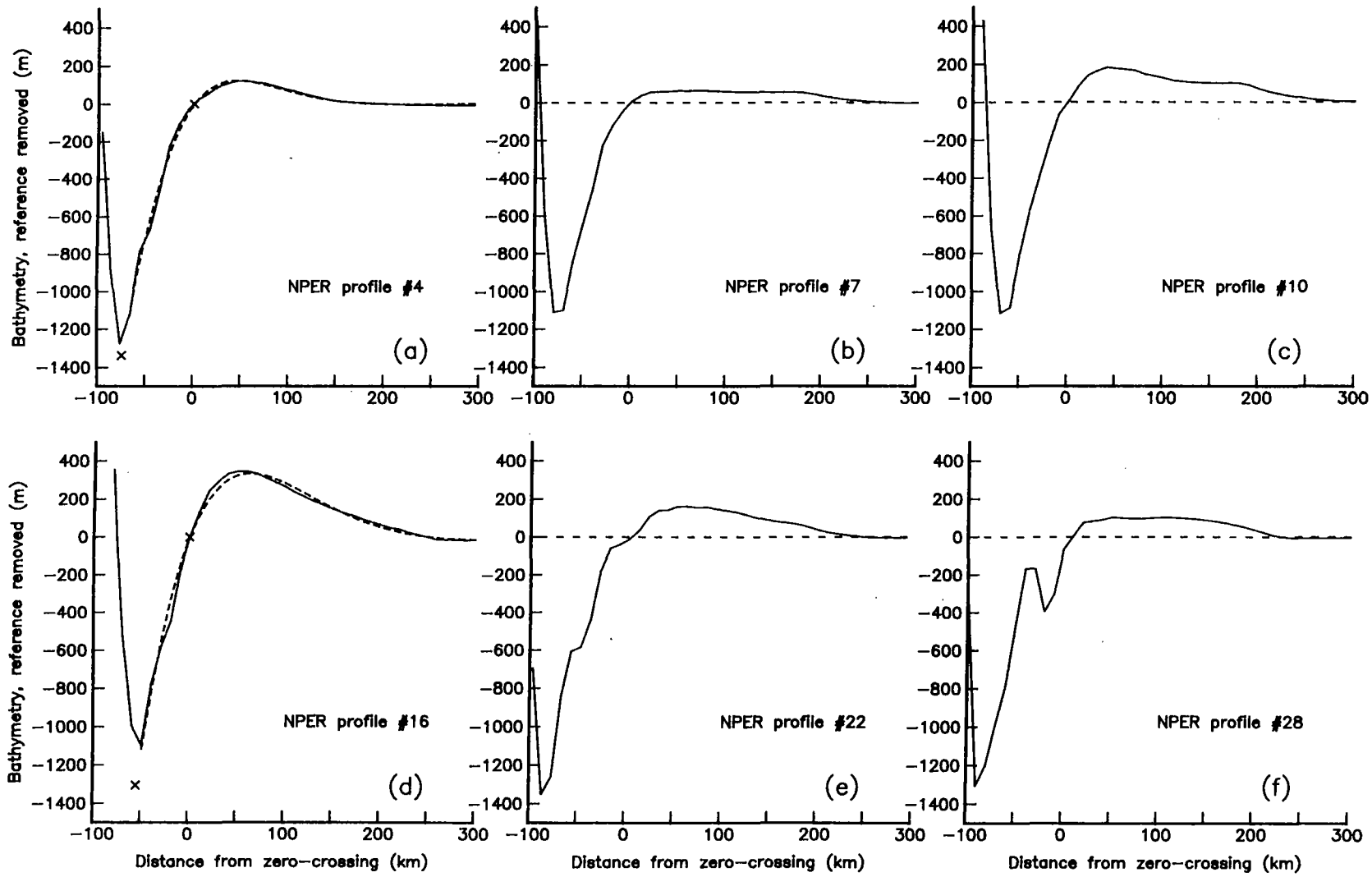
Bathymetry, reference removed (m)
NPER profile #4
(a)
NPER profile #7
(b)
NPER profile #10
(c)
NPER profile #16
(d)
NPER profile #22
(e)
NPER profile #28
(f)
Distance from zero-crossing (km)

Figure 4

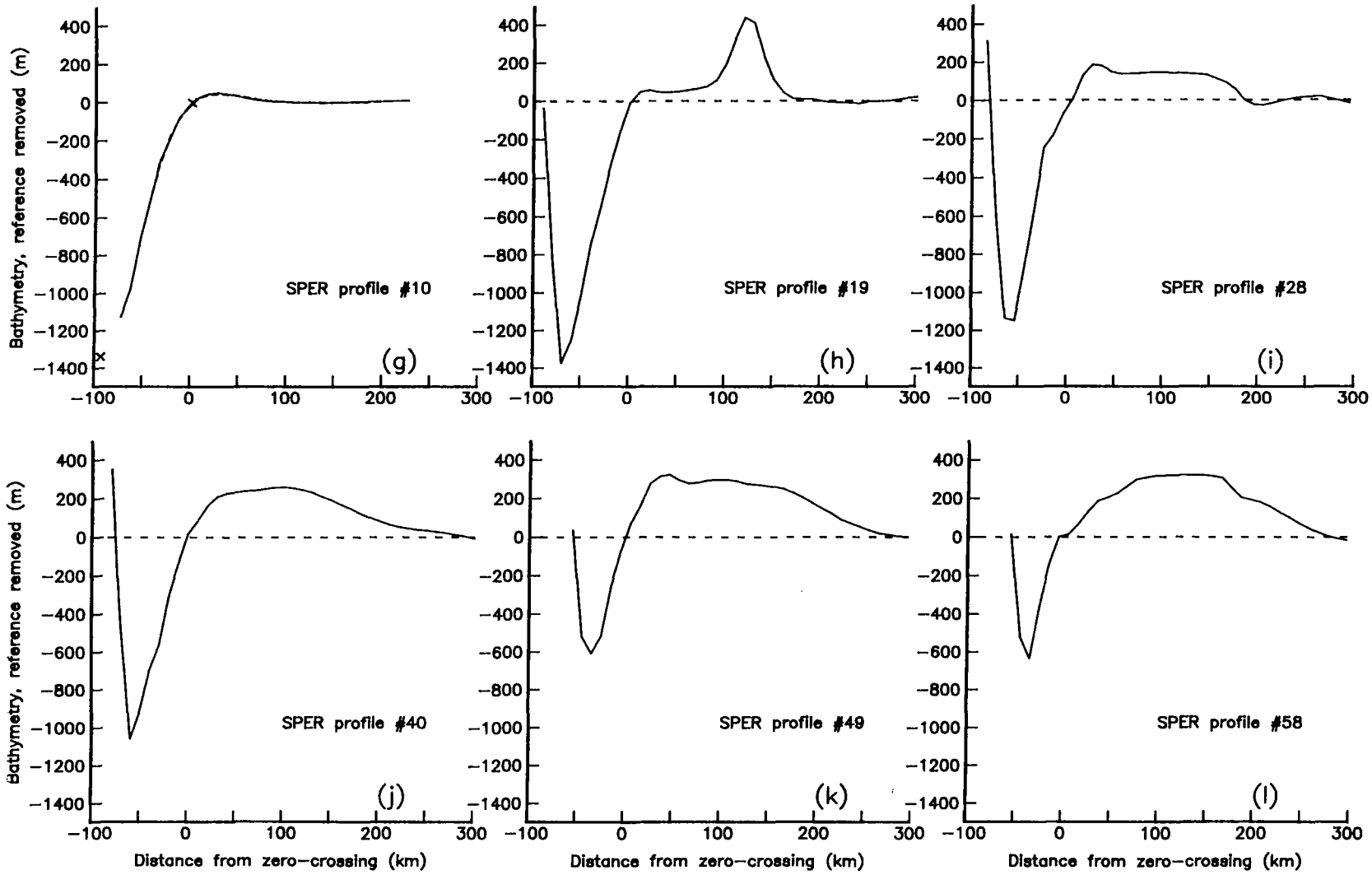
Bathymetry, reference removed (m)
SPER profile #10
(g)
SPER profile #19
(h)
SPER profile #28
(i)
SPER profile #40
(j)
SPER profile #49
(k)
SPER profile #58
(l)
Distance from zero-crossing (km)
Distance from zero-crossing (km)
Distance from zero-crossing (km)

Figure 4

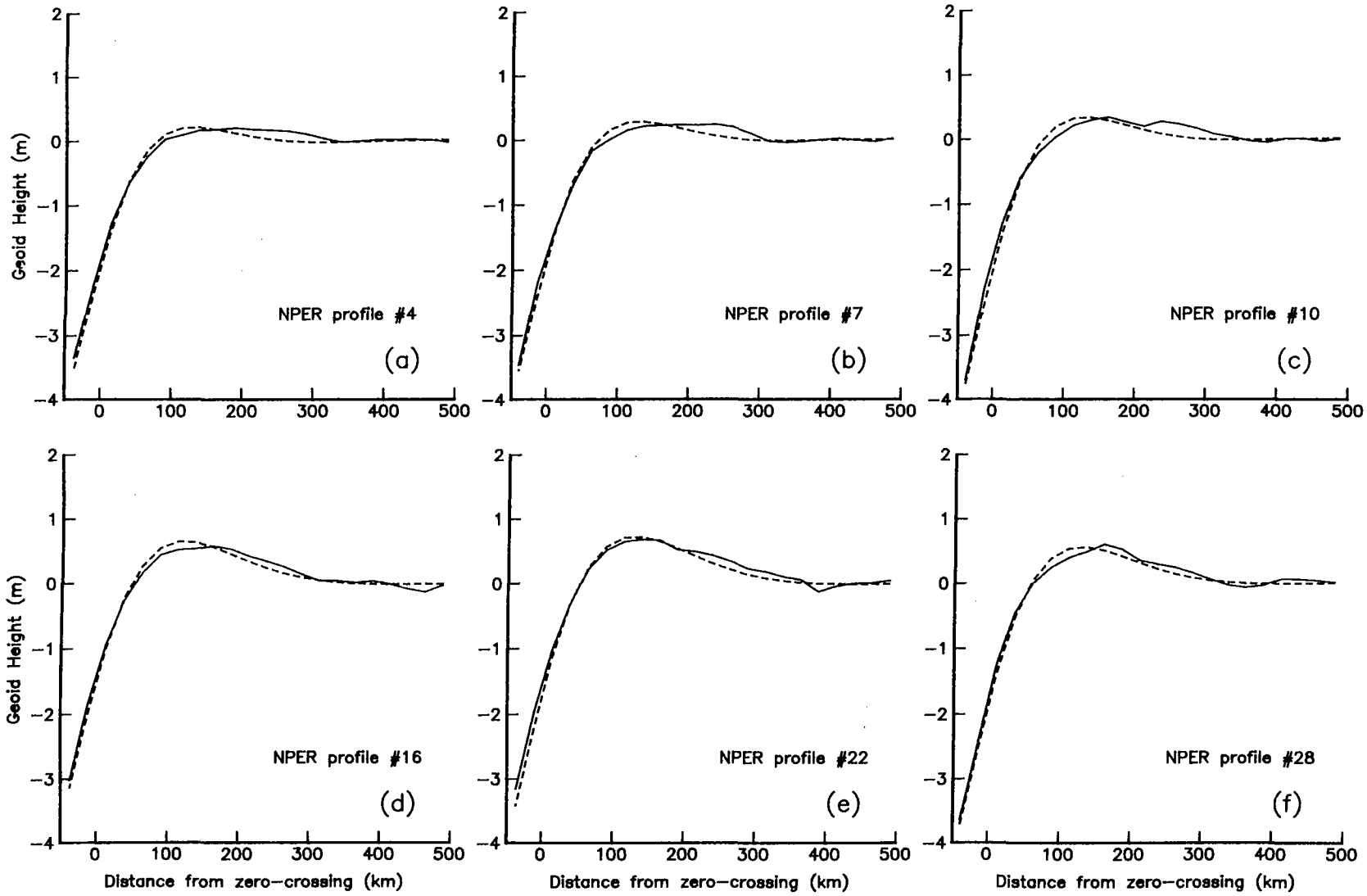
Geoid Height (m)
NPER profile #4
(a)
NPER profile #7
(b)
NPER profile #10
(c)
NPER profile #16
(d)
NPER profile #22
(e)
NPER profile #28
(f)
Distance from zero-crossing (km)
Distance from zero-crossing (km)
Distance from zero-crossing (km)

Figure 5

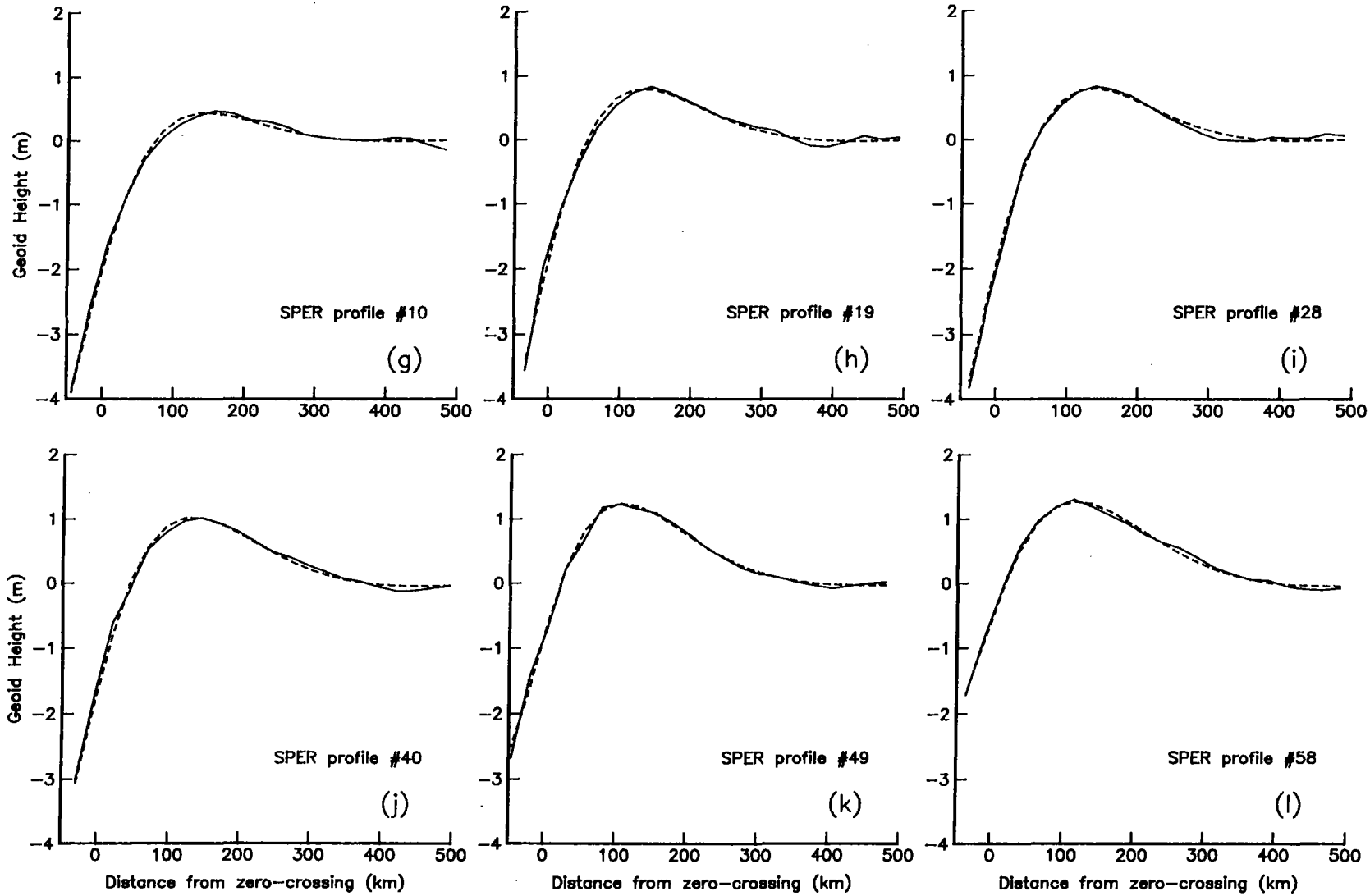
Geoid Height (m)
SPER profile #10
(g)
SPER profile #19
(h)
SPER profile #28
(i)
SPER profile #40
(j)
SPER profile #49
(k)
SPER profile #58
(l)
Distance from zero-crossing (km)
Distance from zero-crossing (km)
Distance from zero-crossing (km)

Figure 5

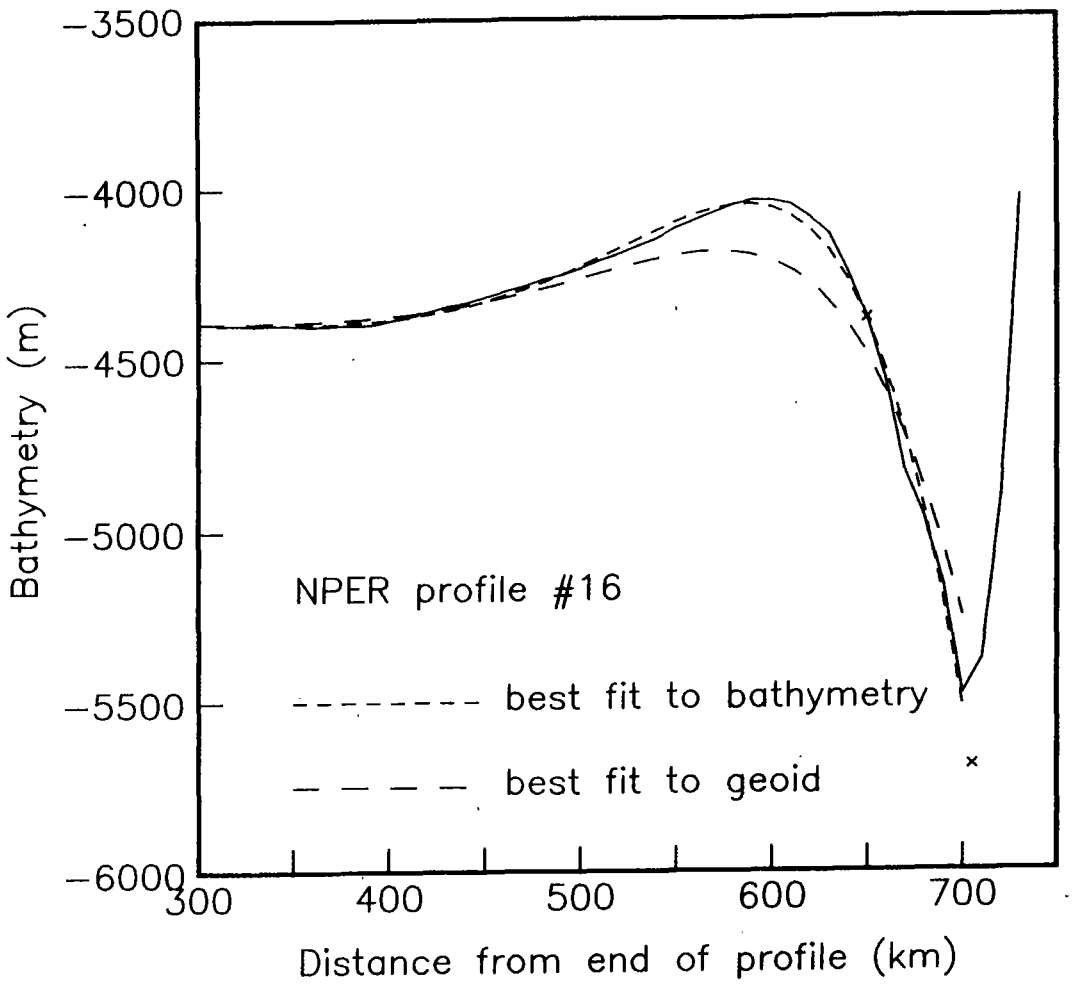
−3500
−4000
−4500
−5000
−5500
−6000
Bathymetry (m)
NPER profile #16
best fit to bathymetry
best fit to geoid
300
400
500
600
700
Distance from end of profile (km)

Figure 6

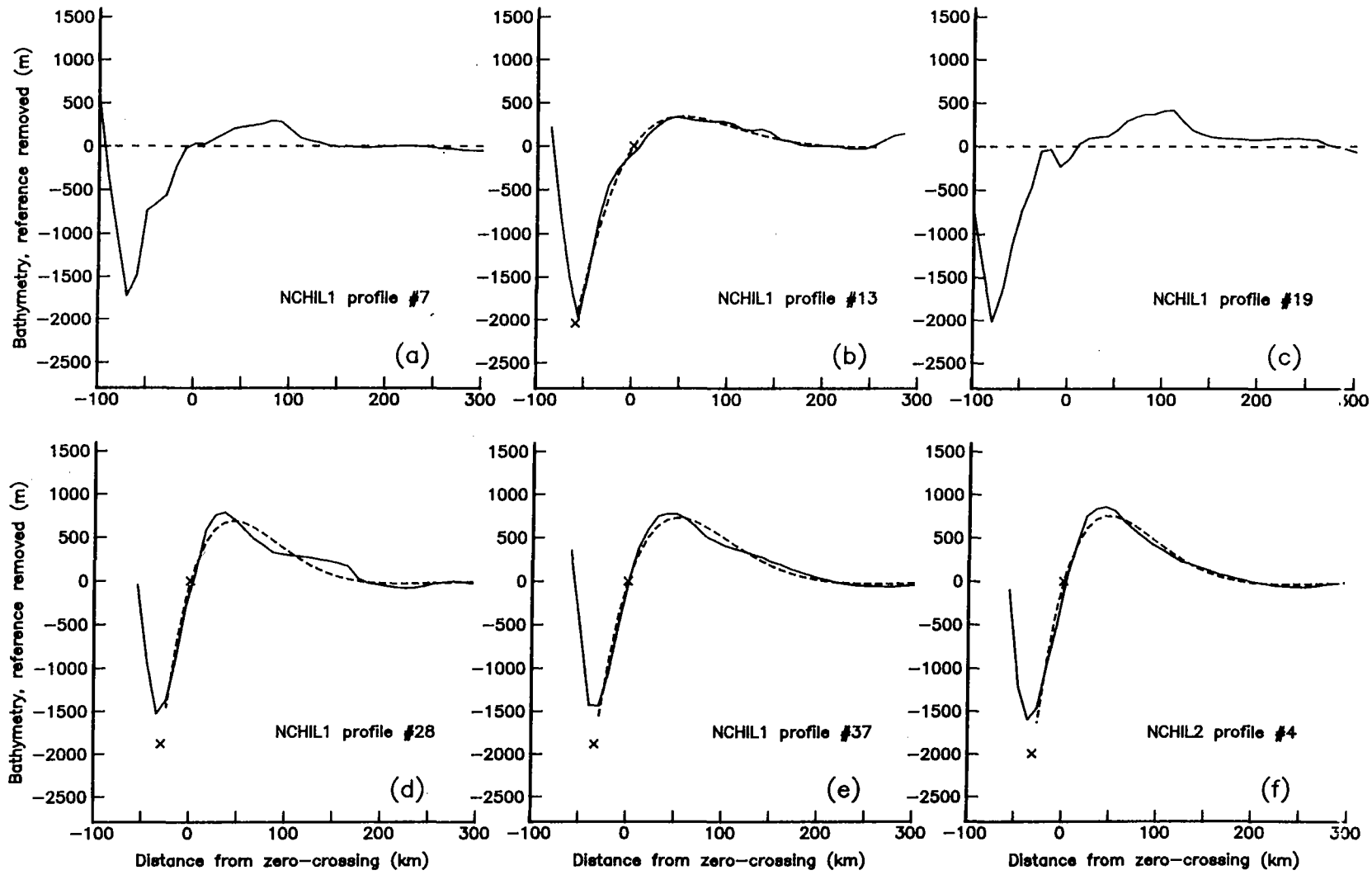
Bathymetry, reference removed (m)
1500
1000
500
0
−500
−1000
−1500
−2000
−2500
−100
0
100
200
300
NCHIL1 profile #7
(a)
NCHIL1 profile #13
(b)
NCHIL1 profile #19
(c)
NCHIL1 profile #28
(d)
NCHIL1 profile #37
(e)
NCHIL2 profile #4
(f)
Distance from zero−crossing (km)

Figure 7

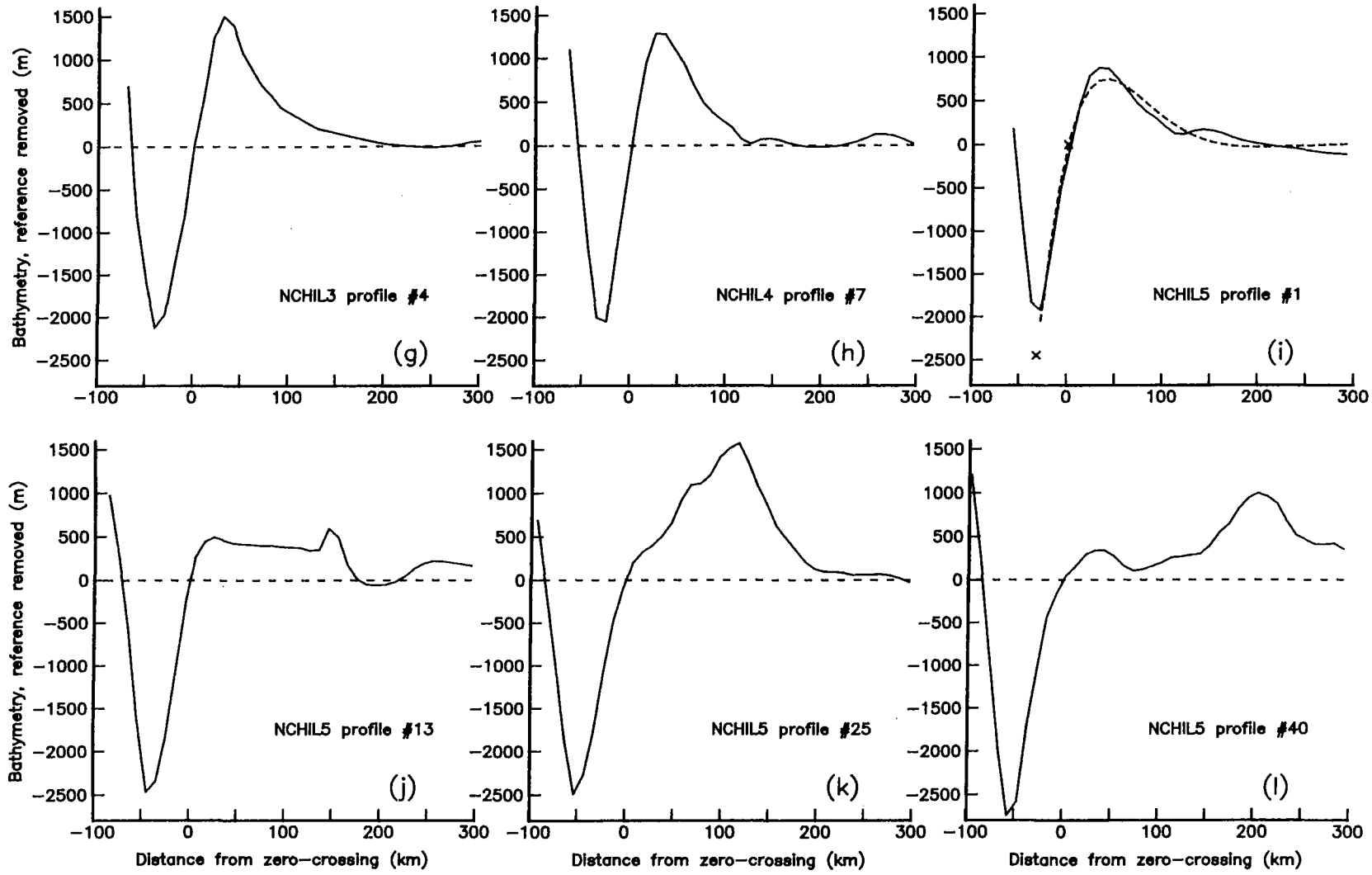
Bathymetry, reference removed (m)
1500
1000
500
0
−500
−1000
−1500
−2000
−2500
−100
0
100
200
300
NCHIL3 profile #4
(g)
NCHIL4 profile #7
(h)
NCHIL5 profile #1
(i)
NCHIL5 profile #13
(j)
NCHIL5 profile #25
(k)
NCHIL5 profile #40
(l)
Distance from zero−crossing (km)

Figure 7

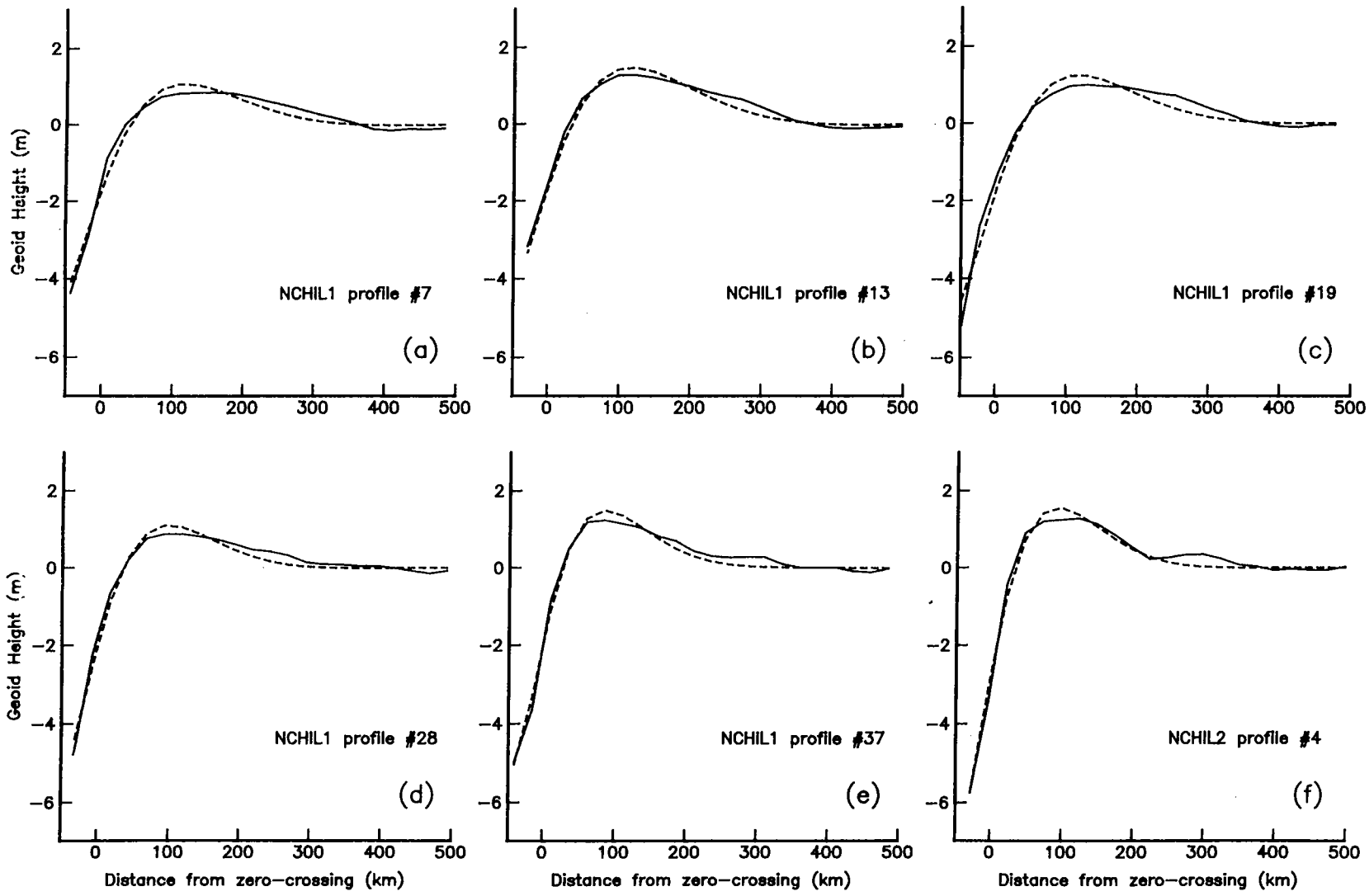
Geoid Height (m)
NCHIL1 profile #7
(a)
NCHIL1 profile #13
(b)
NCHIL1 profile #19
(c)
NCHIL1 profile #28
(d)
NCHIL1 profile #37
(e)
NCHIL2 profile #4
(f)
Distance from zero-crossing (km)

Figure 8

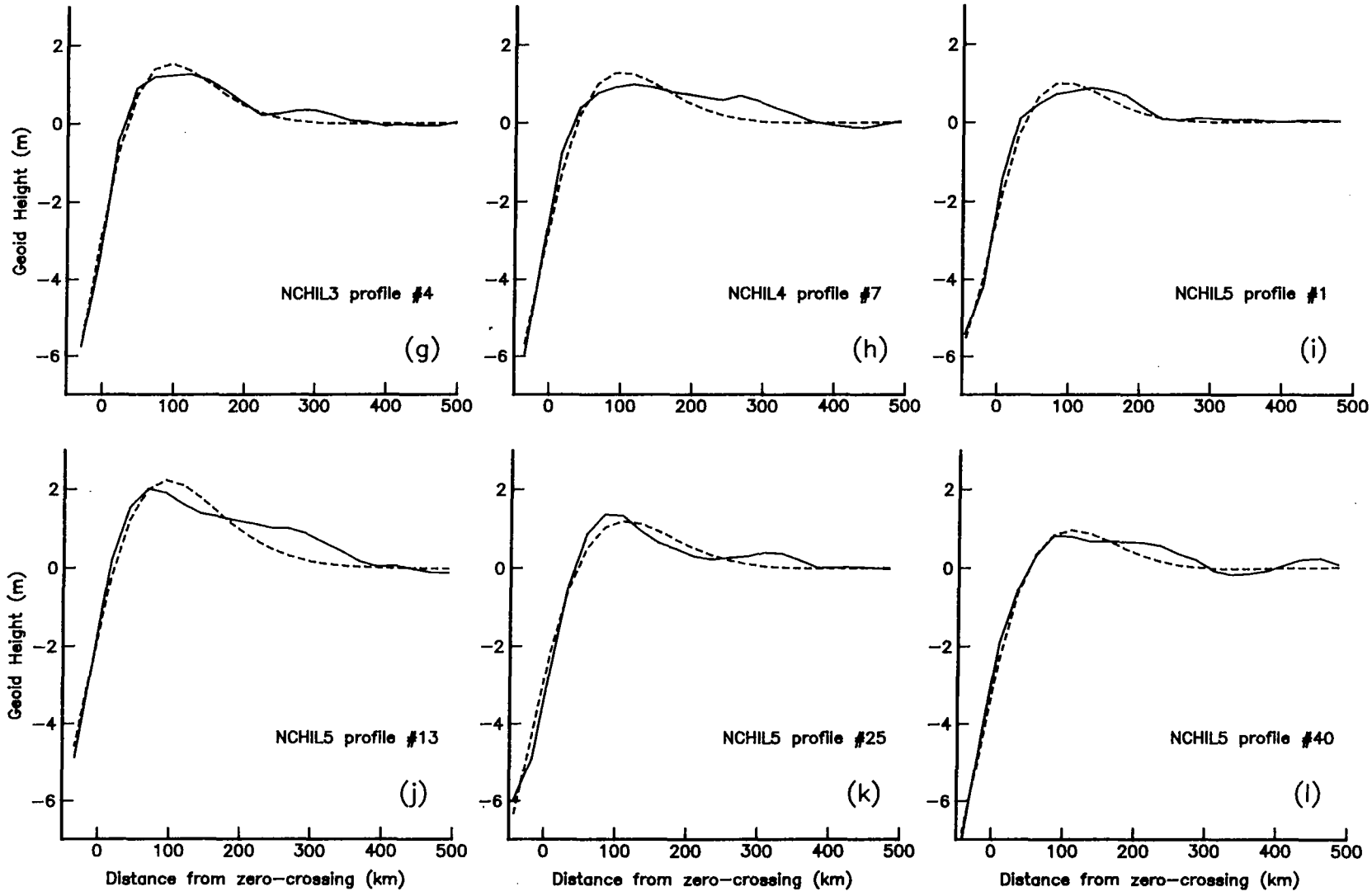
Geoid Height (m)
NCHIL3 profile #4
(g)
NCHIL4 profile #7
(h)
NCHIL5 profile #1
(i)
NCHIL5 profile #13
(j)
NCHIL5 profile #25
(k)
NCHIL5 profile #40
(l)
Distance from zero-crossing (km)
Distance from zero-crossing (km)
Distance from zero-crossing (km)

Figure 8

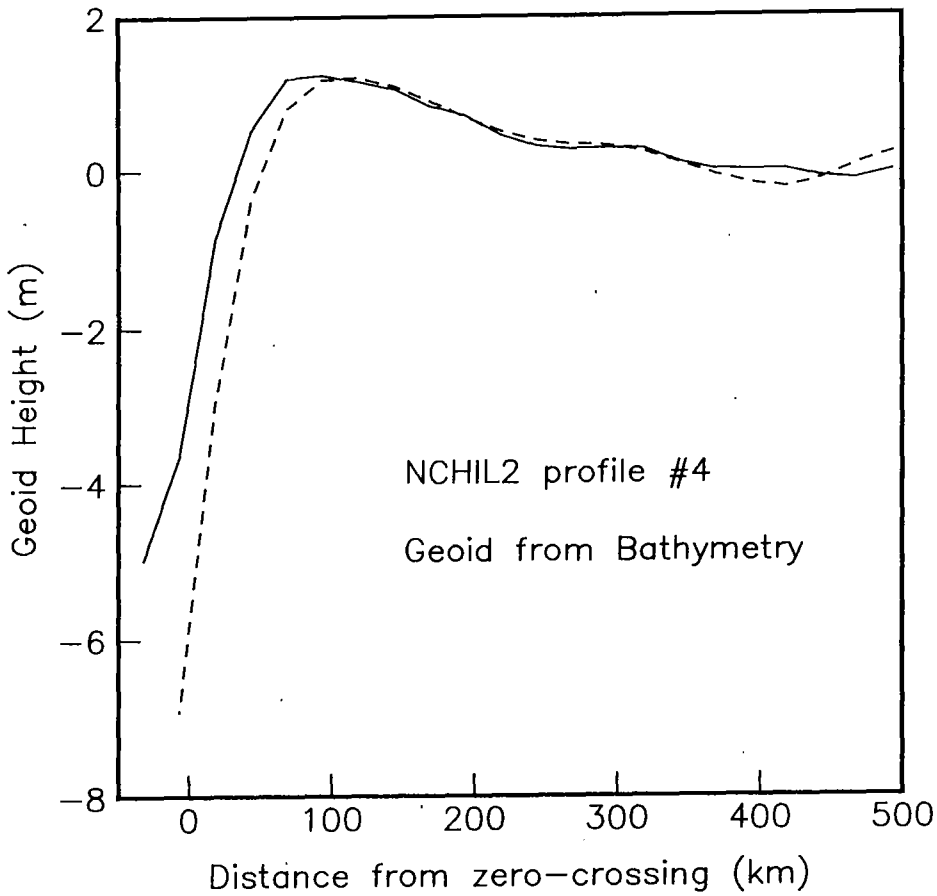
2
0
−2
−4
−6
−8
Geoid Height (m)
NCHIL2 profile #4
Geoid from Bathymetry
0
100
200
300
400
500
Distance from zero−crossing (km)

Figure 9

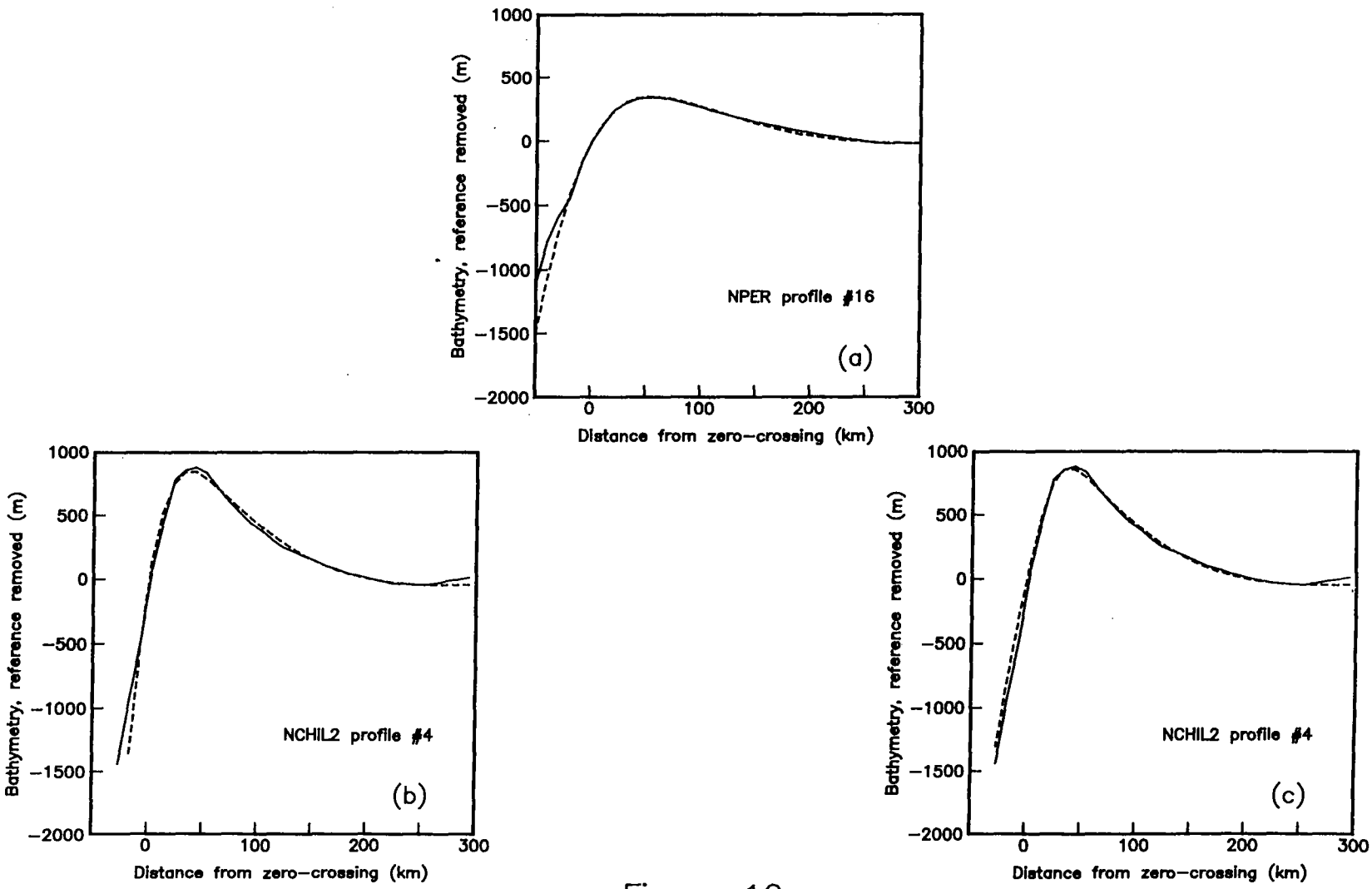
Bathymetry, reference removed (m)
1000
500
0
−500
−1000
−1500
−2000
0
100
200
300
Distance from zero−crossing (km)
NPER profile #16
(a)
NCHIL2 profile #4
(b)
NCHIL2 profile #4
(c)

Figure 10

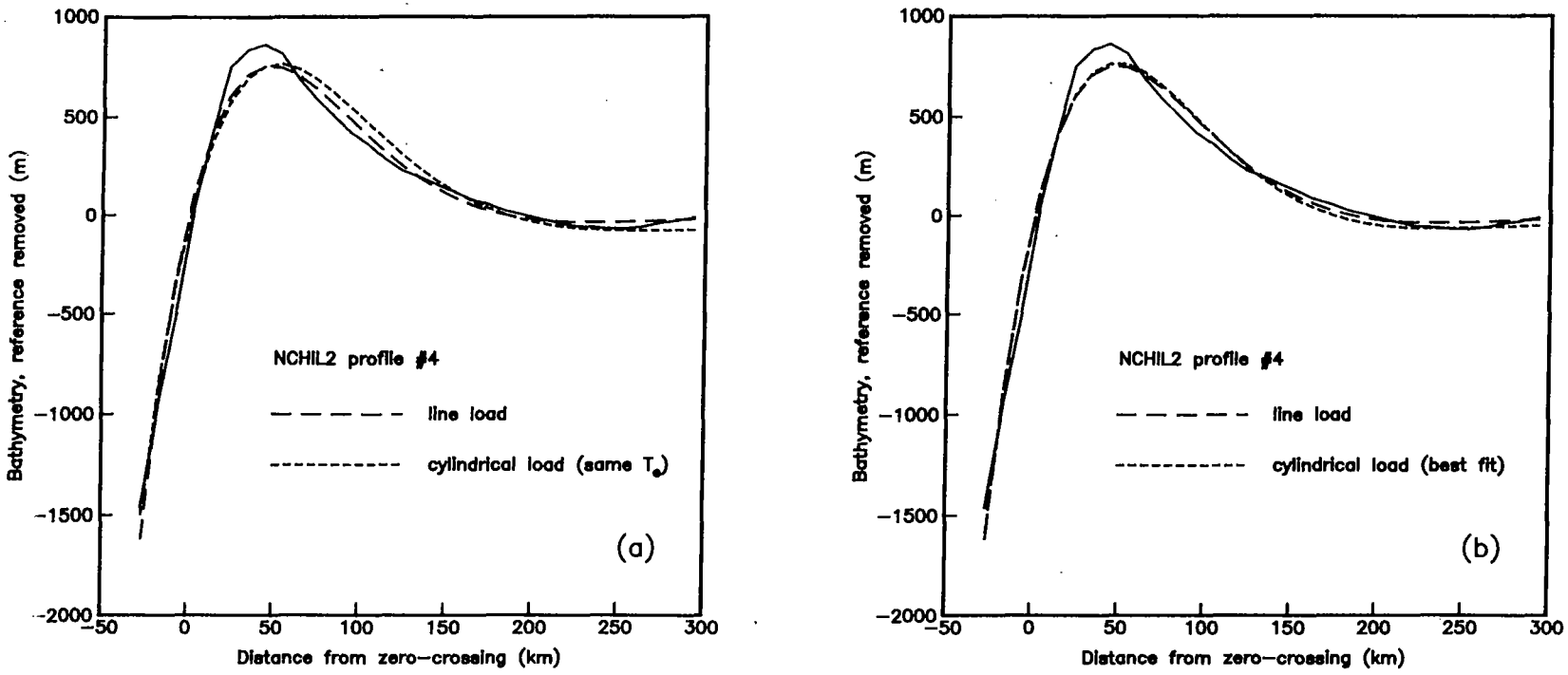
1000
500
0
−500
−1000
−1500
−2000
−50
0
50
100
150
200
250
300
Bathymetry, reference removed (m)
Distance from zero−crossing (km)
NCHIL2 profile #4
line load
cylindrical load (same T_e)
(a)
NCHIL2 profile #4
line load
cylindrical load (best fit)
(b)

Figure 11

Figure 12

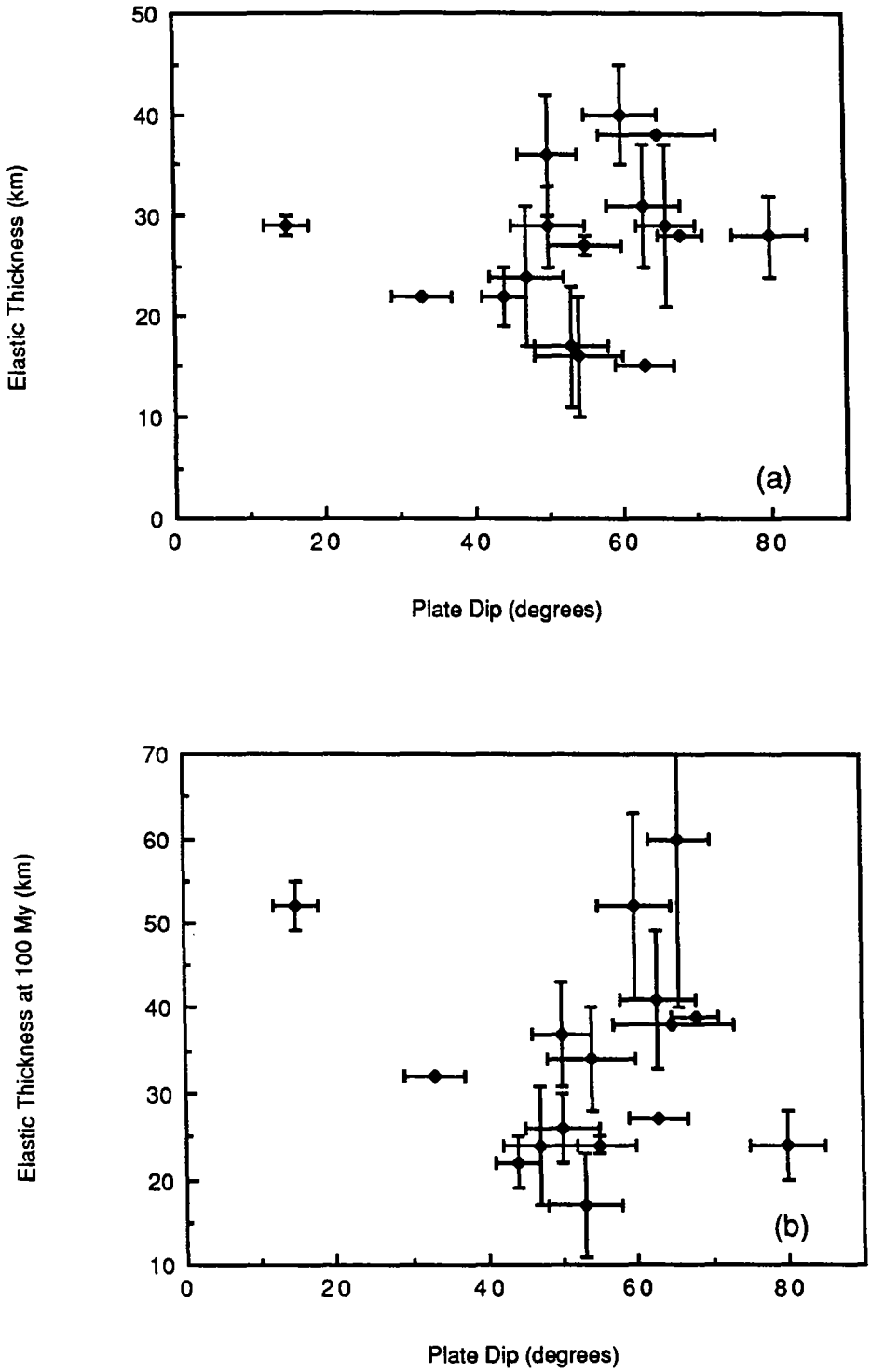
Elastic Thickness (km)
50
40
30
20
10
0
0
20
40
60
80
(a)
Plate Dip (degrees)
Elastic Thickness at 100 My (km)
70
60
50
40
30
20
10
0
20
40
60
80
(b)
Plate Dip (degrees)

Figure 13

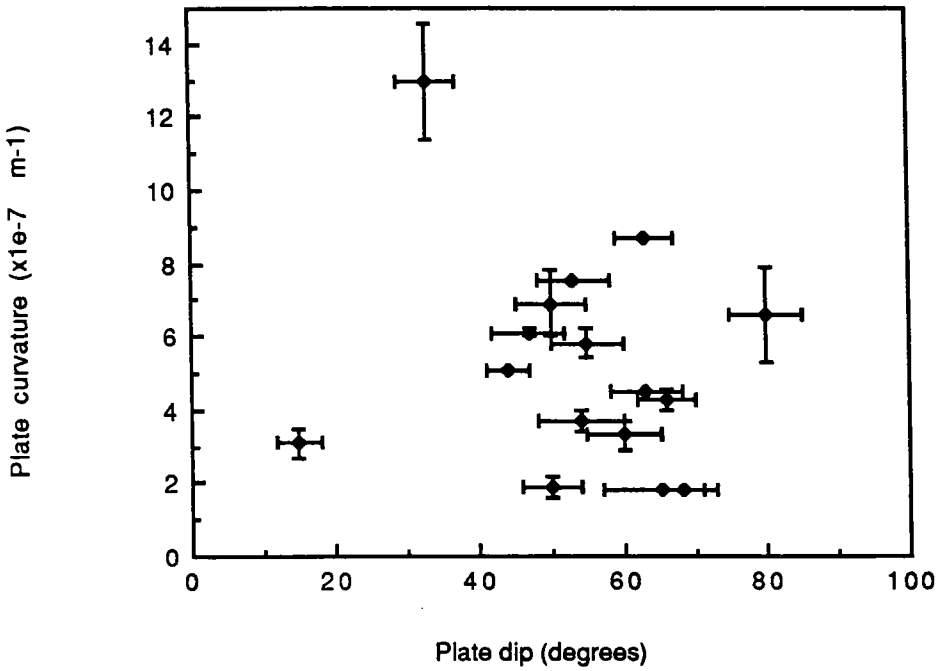
Plate curvature (x1e-7 m-1)
14
12
10
8
6
4
2
0
0
20
40
60
80
100
Plate dip (degrees)

Figure 14

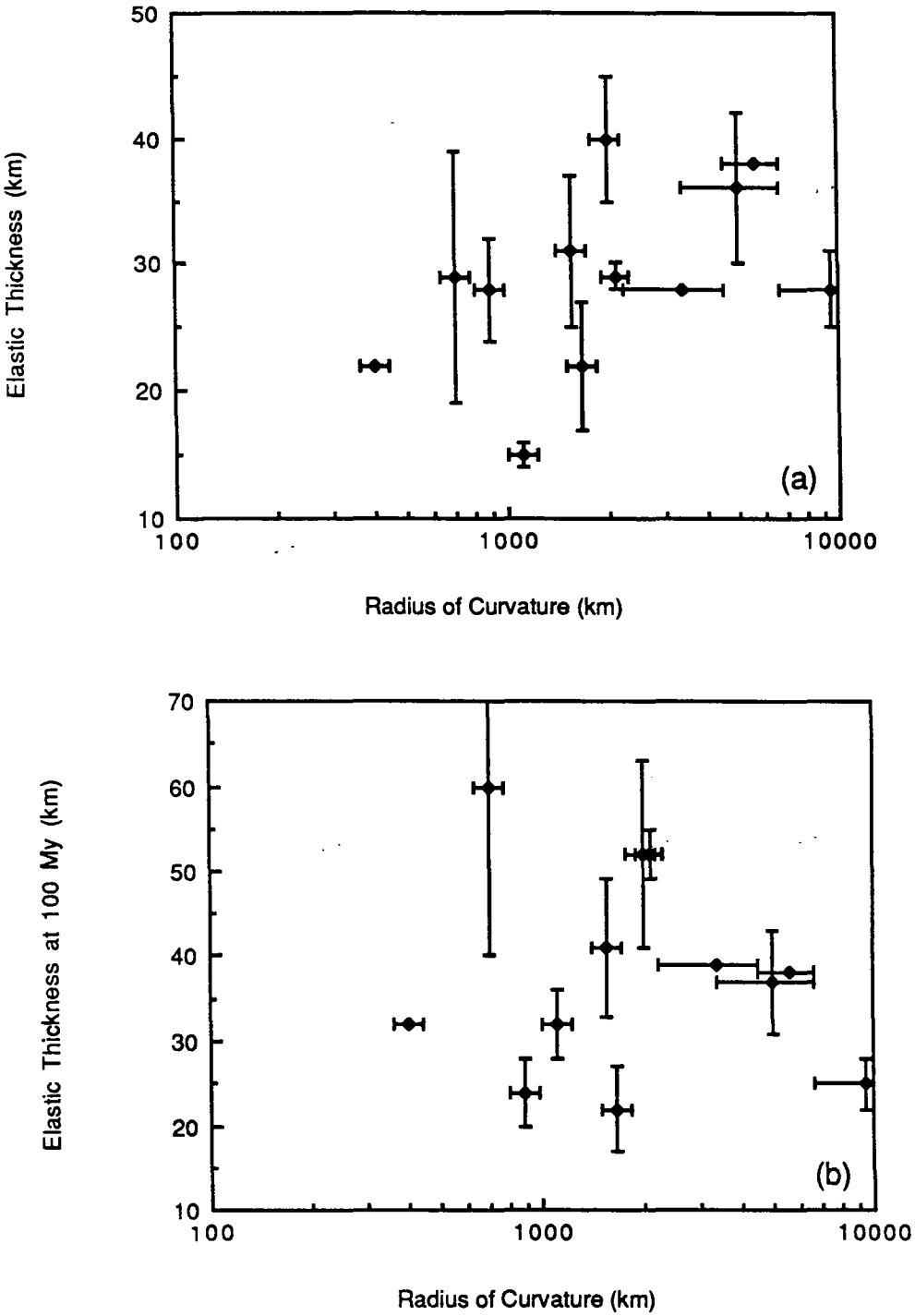
50
40
30
20
10
100
1000
10000
Elastic Thickness (km)
(a)
Radius of Curvature (km)
70
60
50
40
30
20
10
100
1000
10000
Elastic Thickness at 100 My (km)
(b)
Radius of Curvature (km)